
Edge of Stochastic Stability: Revisiting the Edge of Stability for SGD

Arseniy Andreyev^{*1} Pierfrancesco Beneventano^{*1}

Abstract

Recent findings by Cohen et al. (2021) demonstrate that when training neural networks with full-batch gradient descent with step size η , the largest eigenvalue λ_{\max} of the full-batch Hessian consistently stabilizes at $\lambda_{\max} = 2/\eta$. These results have significant implications for convergence and generalization. This, however, is not the case of mini-batch stochastic gradient descent (SGD), limiting the broader applicability of its consequences. We show that SGD trains in a different regime we term Edge of Stochastic Stability (EOSS). In this regime, what stabilizes at $2/\eta$ is *Batch Sharpness*: the expected directional curvature of mini-batch Hessians along their corresponding stochastic gradients. As a consequence, λ_{\max} —which is generally smaller than *Batch Sharpness*—is suppressed, aligning with the long-standing empirical observation that smaller batches and larger step sizes favor flatter minima. We further discuss implications for mathematical modeling of SGD trajectories.

1. Introduction

Training algorithms are a key ingredient to the success of deep learning. Stochastic Gradient Descent (SGD) (Robbins & Monro, 1951), a stochastic variant of Gradient Descent (GD), has been effective in finding parameters that yield good test performance despite the complicated nonlinear nature of neural networks.

In machine learning, full-batch GD and its adaptive versions have been shown to optimize in regime of instability (Xing et al., 2018; Jastrzębski et al., 2019; 2020; Cohen et al., 2021; 2022). Precisely, if the step size is $\eta > 0$ for full-batch GD, the highest eigenvalue of the full-batch Hessian—which we will denote λ_{\max} for simplicity—grows until $2/\eta$ in a first phase of training called progressive sharpening and hovers

right above that value, subject to small oscillations. Cohen et al. (2021) named this regime *Edge of Stability* (EOS). Surprisingly, unlike for quadratics, where this would imply divergence, this instability does not damage convergence when training neural networks.

The work on EOS is about full-batch methods. The picture for full-batch algorithms seems (empirically) clear, both for GD (Cohen et al., 2021; Damian et al., 2023) and its adaptive and accelerated version (Cohen et al., 2022; 2024). Unfortunately, neural networks are typically trained with the mini-batch versions of these gradient-based methods, and how Cohen et al. (2021) in Section 6 and Appendices G and H noticed and stated in the introduction and limitations of their work, what they observed is not the case of mini-batch training. Precisely, to quote Cohen et al. (2021):

while the sharpness does not flatline at any value during SGD (as it does during gradient descent), the trajectory of the sharpness is heavily influenced by the step size and batch size (Jastrzębski et al., 2019; 2020), which cannot be explained by existing optimization theory. Indeed, there are indications that the “Edge of Stability” intuition might generalize somehow to SGD, just in a way that does not center around the sharpness. [...] In extending these findings to SGD, the question arises of how to model “stability” of SGD .

We define here a notion of mini-batch sharpness which acclimates to the learning rate and batch size in a way that mirrors λ_{\max} in the Edge of Stability.

What was empirically known for mini-batch SGD . In the case of mini-batch algorithms, (i) Jastrzębski et al. (2019; 2020) noticed that for SGD the phase transition happens earlier for smaller η or smaller batch size b , but they did not quantify when. Moreover, Cohen et al. (2021) noticed that SGD somehow acclimates to the hyperparameters. However, they did not characterize how, if not negatively, (ii) it seems not to “flatline” at any value of λ_{\max} and (iii) if it stabilizes, that always happens at a level they could not quantify which is below the $2/\eta$ threshold, see Figure 1, often without a proper progressive sharpening phase. This scenario leaves the most basic questions open: *In what way the location*

^{*}Equal contribution. ¹Princeton University, Princeton, NJ, USA. Correspondence to: Arseniy Andreyev <andreyev@princeton.edu>, Pierfrancesco Beneventano <pierb@princeton.edu>.

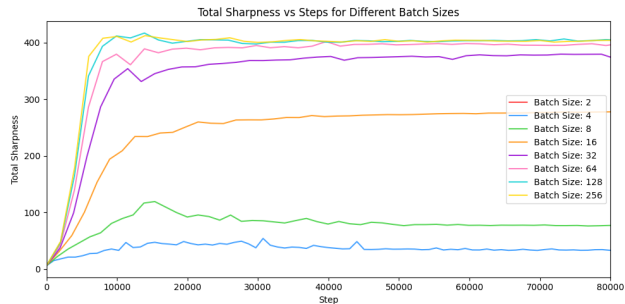


Figure 1. Mini-batch SGD on CIFAR-10. The full-batch Hessian’s largest eigenvalue λ_{\max} typically plateaus below $2/\eta$, here $\eta = 1/200$. Smaller batch sizes lead to lower plateau values.

of convergence of SGD acclimates to the choice of hyper-parameters? What are the key quantities involved? To be more specific, can we characterize the training phenomena in (i), (ii), (iii) above? What determines them? Does SGD train in an unstable regime?

Edge of Stochastic Stability. We address the questions above by introducing a general framework for SGD dynamics through the concept of *Batch Sharpness*: the expectation of the Hessians of mini-batch losses along the direction of the mini-batch gradients, see Section 3.1. This serves as a generalized and direct substitute for λ_{\max} in the mini-batch SGD setting. Specifically, we identify a new regime—which we term *Edge of Stochastic Stability* (EoSS)—where *Batch Sharpness* stabilizes near $2/\eta$, while maintaining a critical gap with λ_{\max} . This dynamic explains the plateaus of λ_{\max} at lower levels determined by batch size and learning rate, unifying the observed phenomena in mini-batch training.

Organization of the rest of the paper. Section 2 reviews related work and outlines key open questions. In Section 3, we introduce and empirically validate the phenomenon of Edge of Stochastic Stability. Section 4 discusses what the observed notion of stability entails mathematically. In Section 5, we examine stability mathematically and we study values at which λ_{\max} plateaus. In Section 6, we discuss the implications for the structure and modeling of SGD dynamics. Finally, Section 7 summarizes our findings and addresses the limitations of this work.

2. Related Work

2.1. Progressive Sharpening and Edge of Stability

Progressive sharpening. Early work noticed that the local shape of the loss landscape changes rapidly at the beginning of the training (LeCun et al., 2012; Keskar et al., 2016; Achille et al., 2017; Jastrzębski et al., 2018; 2019; Fort & Ganguli, 2019). Multiple papers noticed growth of different

estimators of λ_{\max} in the early training (Keskar et al., 2016; Sagun et al., 2016; Fort & Scherlis, 2019; Jastrzębski et al., 2019). Later, Jastrzębski et al. (2019; 2020) and Cohen et al. (2021) managed to make this precise, noticing that, along the trajectories of SGD and GD, λ_{\max} increases steadily, often after a small number of steps of decrease. This phenomenon was called progressive sharpening by Cohen et al. (2021).

A phase transition. Early studies (Goodfellow et al., 2016; Li et al., 2019; Jiang et al., 2019; Lewkowycz et al., 2020) revealed that large initial learning rates often enhance generalization at the cost of initial loss reduction. Jastrzębski et al. (2020) attributed this to a sudden phase transition, termed the break-even point, marking the end of progressive sharpening. This transition slows the convergence by confining the dynamics to a region of lower sharpness. Unlike progressive sharpening, this phenomenon is considered to be induced by the gradient-based algorithm becoming unstable, not by the landscape. Jastrzębski et al. (2019; 2020); Cohen et al. (2021; 2022) indeed showed that the phase transition comes at different points for different algorithms on the same landscapes. Jastrzębski et al. (2019; 2020) showed that in the case of mini-batch SGD this phase comes earlier for bigger step sizes and smaller batch sizes, without quantifying it. Cohen et al. (2021; 2022) later showed indeed that it comes at the instability thresholds for the full-batch optimization algorithms.

Full-batch edge of stability. After the phase transition above, GD and full-batch Adam train in the EOS oscillatory regime (Cohen et al., 2021; 2022), where the λ_{\max} stabilizes and oscillates around a characteristic value. The name is due to the fact that, in the case of full-batch GD, the λ_{\max} hovers at $2/\eta$ which is the stability threshold for optimizing quadratics. Observations from Cohen et al. (2021; 2022) indicate that most training dynamics occur within this regime, effectively determining λ_{\max} of the final solution. Lee & Jang (2023) explained why λ_{\max} in this regime is generally above $2/\eta$, rarely aligning exactly. The reasons include: (i) nonlinearity of the loss gradient, which shifts the required value depending on higher-order derivatives, and (ii) the EOS being governed by the Hessian along the gradient direction, rather than λ_{\max} alone.

EoS and convergence. There is a growing body of work analyzing the surprising mechanism of EOS in training dynamics with GD. Classically, when gradients depend linearly on parameters, divergence occurs locally if $\eta > \frac{2}{\lambda}$, as demonstrated with one-dimensional parabolas (Cohen et al., 2021). Yet, neural networks often converge even when $\eta \geq \frac{2}{\lambda}$, likely due to the problem’s non-standard geometry. Damian et al. (2023) proposed an explanation under some, empirically tested, assumptions of alignment of third derivatives and gradients. Wang et al. (2022) showed that the

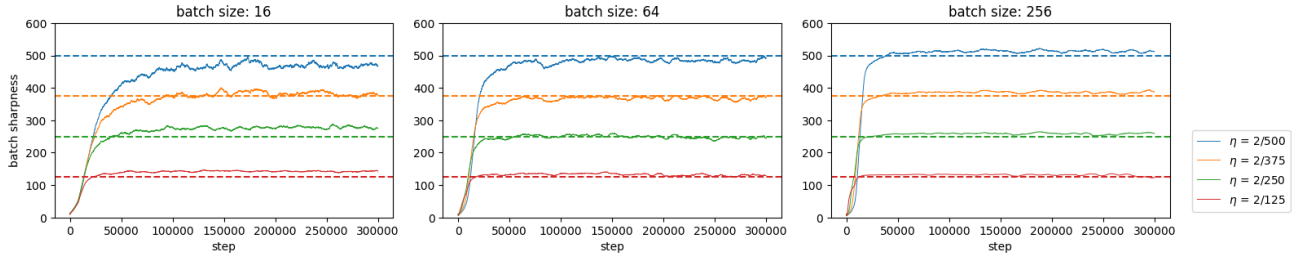


Figure 2. **SGD at EoSS under different learning rates and batch sizes.** We train a fully-connected network on an 8k subset of CIFAR-10. *Batch Sharpness* stabilizes at the $2/\eta$ threshold across varying batch sizes and step sizes.

product-like structure of shallow networks guarantees convergence with learning rates exceeding the EOS threshold. Beneventano & Woodworth (2025) showed that although convergence is guaranteed, it may be extremely slow, this may, however, benefit implicit regularization effects. For further exploration of convergence and implicit regularization in the EOS regime, we direct the reader to Arora et al. (2022); Ahn et al. (2022; 2023); Zhu et al. (2023); Lyu et al. (2023).

2.2. SGD, Hessian, and Generalization

SGD finding flatter minima. Our result is inherently a result about mini-batch training improving flatness. Specifically, we explain why:

Training with smaller batches constrains the dynamics in areas with smaller eigenvalues for the full-batch Hessian.

This quantifies and characterizes prior observations that SGD tends to locate flat minima (Hochreiter & Schmidhuber, 1997) and that smaller batch sizes result in reduced Hessian sharpness (Keskar et al., 2016). Analogously, recent work strongly aligns with our result: Jastrzębski et al. (2021) demonstrates that large learning rates in SGD act similarly to penalizing the trace of the Fisher matrix—which approximates the Hessian during training and shares its top eigenspaces (Jastrzębski et al., 2018; Martens, 2020; Thomas et al., 2020)—in image classification tasks.

Sharpness and Generalization. SGD-trained networks consistently generalize better than GD-trained ones, with smaller batch sizes further enhancing generalization performance (LeCun et al., 2012; Keskar et al., 2016; Goyal et al., 2017; Jastrzębski et al., 2018; Masters & Luschi, 2018; Smith et al., 2021). This advantage has been widely attributed to the flatness of the minima (Murata et al., 1994; Hochreiter & Schmidhuber, 1994; Neyshabur et al., 2017; Wu et al., 2017; Dinh et al., 2017; Kleinberg et al., 2018; Jiang et al., 2019; Xie et al., 2020). Training algorithms explicitly designed to find flat minima have indeed demon-

strated strong performance across various tasks (Izmailov et al., 2019; Foret et al., 2021). Moreover, Jastrzębski et al. (2021) shows that, in practice, penalizing the trace of the Fisher information matrix empirically improves generalization and reduces memorization—especially when training with noisy labels. We believe that our quantification and the introduction of a theoretical framework for these improvements in sharpness may be a stepping stone towards understanding these generalization benefits theoretically.

3. SGD Typically Occurs at the EoSS

Extending Cohen et al. (2021), we identify a stable quantity in mini-batch SGD: *Batch Sharpness*. We empirically demonstrate that SGD operates in a regime we term Edge of Stochastic Stability, observed across multiple datasets and architectures. *Batch Sharpness* emerges as the key quantity governing this regime, serving as the analogous for mini-batch training of the sharpness.

3.1. Mini-Batch Sharpness

Let $L_B(\theta) = \frac{1}{b} \sum_{(x_i, y_i) \in B} \tilde{L}(f_\theta(x_i), y_i)$ be the empirical loss on a randomly sampled batch B of size b . Denote by $\mathcal{H}(L_B)$ the Hessian w.r.t. θ of L_B , and let $\nabla L_B(\theta)$ be its gradient. We define:

Definition 1 (*Batch Sharpness*). Let \mathcal{P}_b be the distribution of random batches of size b . The *Batch Sharpness* is

$$\text{Batch Sharpness} = \frac{\mathbb{E}_{B \sim \mathcal{P}_b} [\nabla L_B^\top \mathcal{H}(L_B) \nabla L_B]}{\mathbb{E}_{B \sim \mathcal{P}_b} [\|\nabla L_B\|^2]}.$$

Denote by $\lambda_{\max} := \lambda_{\max}[\mathcal{H}(L)]$ the largest eigenvalue of the Hessian of the full-batch loss. While *Batch Sharpness* behaves as λ_{\max} in EOS, the two quantities differ fundamentally. We explore this distinction further in Section 4.

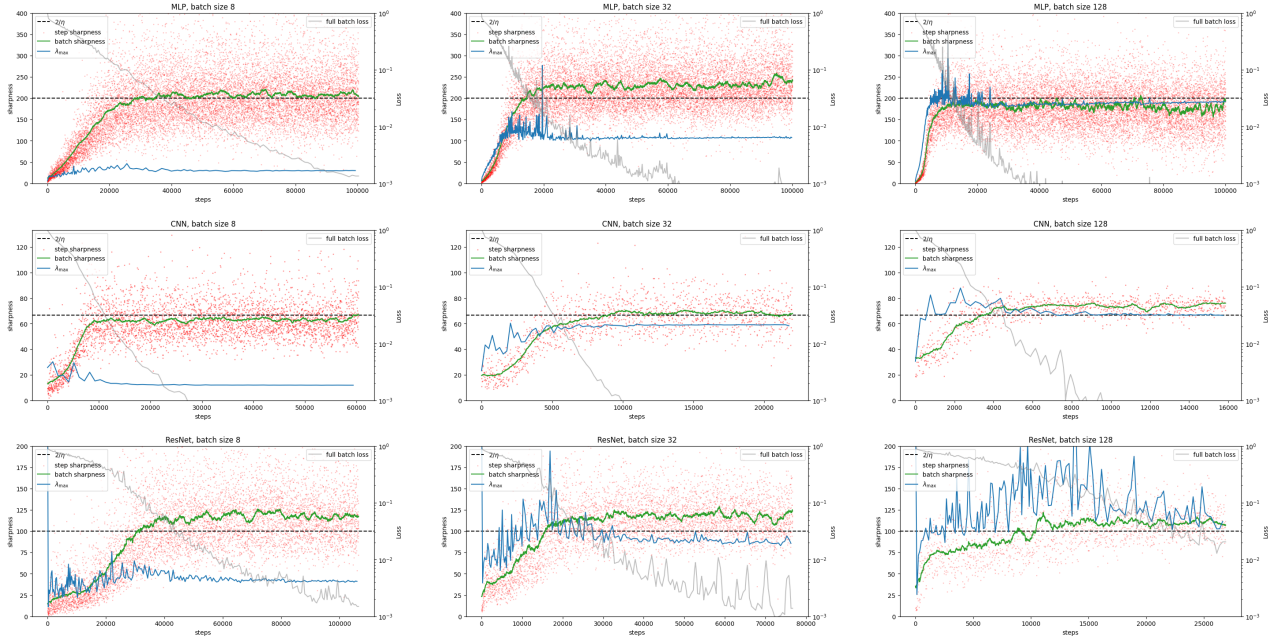


Figure 3. Comparing different sharpness measures. Red: observed sharpness on the step’s mini batch on the batch used for the step; Green: average *Batch Sharpness* (Definition 1); Blue: full-batch λ_{\max} . Top row: MLP (2 hidden layers of width 512); middle: 5-layer CNN; bottom: ResNet-14; all trained on an 8k subset of CIFAR-10.

3.2. The Edge of Stochastic Stability

1. Stabilization of *Batch Sharpness*: We establish that SGD operates in a stability regime analogous to EOS, which we term *Edge of Stochastic Stability*. In this regime *Batch Sharpness* stabilizes at $2/\eta$:

SGD tends to train in an instability regime we call Edge of Stochastic Stability. Precisely, after a phase of progressive sharpening, Batch Sharpness reaches a stability level of $2/\eta$, and hovers there.

2. Stabilization of λ_{\max} : Also λ_{\max} typically stabilizes. However, it does so at lower values that depends on the trajectory taken (Figures 3 and 5). We discuss the stabilization level of λ_{\max} in Section 3.3 and 5. Consequently, standard EOS analysis that relies solely on λ_{\max} cannot explain SGD’s actual training behavior in the small-batch setting.

3. Catapults: Unlike EOS, EOSS stabilizes the expectation of a quantity which the algorithm sees one observation at time. Occasionally, a series of batches sampled have outlying sharpness—that is too high for the stable regime—and steps overshoot, triggering a catapult effect, where *Batch Sharpness* spikes before rapidly decreasing (Figure 4). This is typically followed by renewed progressive sharpening, returning to the EOSS regime. This results in a catapult phase for the training loss, aligning with, and maybe explaining, previous observations about catapult behaviors, see, e.g.,

Lewkowycz et al. (2020); Zhu et al. (2024).

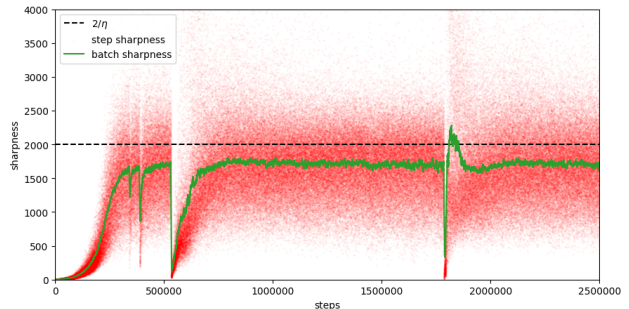


Figure 4. Catapults during EOSS. During EOSS, *Batch Sharpness* may through cycles of progressive sharpening and stabilizations. Red dots are the observed sharpnesses of the batches used for the step, the green line is *Batch Sharpness*.

3.3. *Batch Sharpness* Governs EOSS

Following Cohen et al. (2021) we show here how the dynamics of *Batch Sharpness* changes when hyper-parameters shift along the dynamics. Interestingly, while λ_{\max} and other full-batch Hessian metrics may stabilize, we show here their specific plateaus or trajectories depend on initial conditions, not only on the hyperparameter. By contrast, $\lambda_{\max}(\mathcal{H}(L_B))$ —the top eigenvalue of the *mini-batch* Hessian—does consistently stabilize and shift with hyperparameters.

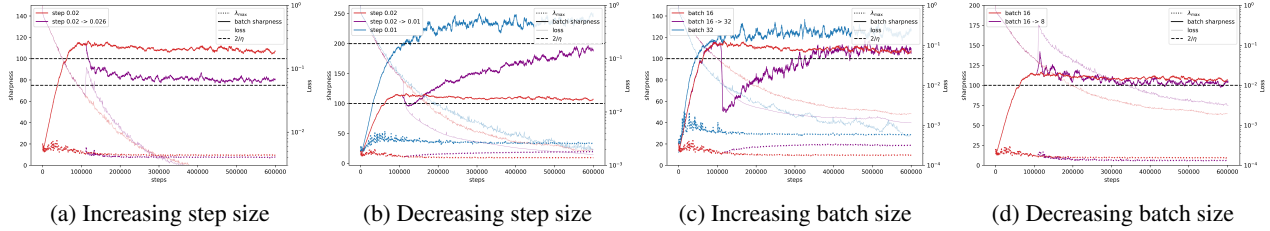


Figure 5. Effects of changing step size or batch size in EOSS. (a) Increasing the learning rate causes a catapult spike before *Batch Sharpness* settles at the new $2/\eta$. (b) Decreasing the learning rate prompts renewed progressive sharpening. (c) Increasing the batch size narrows the gap between *Batch Sharpness* and λ_{\max} . (d) Decreasing the batch size. Triangles mark the steps at which the hyperparameters were changed.

Changing the step size. Increasing the step size η triggers a *catapult* spike in all the quantities in considerations and the training loss, before *Batch Sharpness* re-stabilizes near the updated threshold $2/\eta$ (Fig. 5a). This therefore pushes λ_{\max} lower. Crucially, if stability was governed solely by λ_{\max} , this step-size adjustment would have left the dynamics unchanged, as λ_{\max} remains below both the original and revised $2/\eta$ thresholds. Conversely, reducing η (Fig. 5b) raises the $2/\eta$ threshold and prompts a new phase of progressive sharpening of *Batch Sharpness*. Here, λ_{\max} also rises, but ultimately stabilizes at a lower value than if the entire training had run with the smaller step size. Again, if stability was governed solely by λ_{\max} , this step-size adjustment would have had the same effect as starting from scratch with the new step size. Notably, *Batch Sharpness* initially decreases—a counterintuitive result potentially linked to shifting alignments between gradients and Hessian eigenvectors. This behavior warrants further investigation.

Changing the batch size. Increasing the batch size reduces the gap between *Batch Sharpness* and λ_{\max} , therefore making *Batch Sharpness* lower, (Fig. 5c), and thus below the $2/\eta$ threshold. This causes a new progressive sharpening phase until *Batch Sharpness* again reaches the $2/\eta$ level, making λ_{\max} stabilize at a new, higher level, again lower than the one of the training started from scratch with the new batch size. This shows that it is indeed the *Batch Sharpness* that is the "limiting" quantity in EOSS. Conversely, decreasing the batch size induces a brief catapult phase, after which *Batch Sharpness* returns to its previous plateau, as expected. This forces full-batch λ_{\max} to adjust to a lower level.

Overall, we find that *Batch Sharpness* governs EOSS behavior—mirroring how λ_{\max} operates in the full-batch EOS—while the actual full-batch λ_{\max} lags behind or settles inconsistently, underlining the mini-batch nature of SGD stability.

4. Mathematics of Stability

It may seem surprising at first that *Batch Sharpness* is not a quantity of the same nature as λ_{\max} or is not a function of the full-batch Hessian. The reason is deep into the nature of mini-batch SGD. After recalling the computations of Cohen et al. (2021) in Section 4.1, we show what is the setting of mini-batch SGD and what is the notion of stability which depends on *Batch Sharpness* in Section 4.2. Later in Section 4.3 we motivate why the stability of mini-batch SGD, surprisingly, can not depend on full-batch quantities.

4.1. A Quadratic Objective: Full-Batch GD

We recall here the arguments of Cohen et al. (2021) and Lee & Jang (2023) for quadratic objective functions to later show how stability differs between the two settings.

Assume we fix a learning rate η for the whole training. Consider the example of the quadratic Taylor approximation of a loss function:

$$f(x) = \frac{1}{2}x^\top \mathbf{A}x + \mathbf{b}^\top x + \mathbf{c},$$

where \mathbf{A} is the Hessian matrix (symmetric and positive semidefinite), \mathbf{b} is the gradient vector, and \mathbf{c} is a constant. Here, as Cohen et al. (2021) observed, when $\eta\lambda_{\max}(\mathbf{A}) > 2$ the component of $x_t - x^*$ parallel to the eigenvector relative to $\lambda_{\max}(\mathbf{A})$ explodes with a power law. This is equivalent to imposing the inequality (1) *at every step*.

$$-\eta\|\nabla f(x_t)\|^2 + \frac{\eta^2}{2}\nabla f(x_t)^\top \mathbf{A}\nabla f(x_t) \leq 0, \quad (1)$$

Indeed, eventually, we have $f(x_{t+1}) > f(x_t)$, i.e., if and only if $\lambda_{\max} \leq 2/\eta$.

4.2. Quadratic Objectives: Mini-Batch GD

Empirically, progressive sharpening halts when the mini-batch analog of (1) reaches zero in expectation. Concretely, EOSS arises if, at *each step*,

$$\eta\|\nabla f_B(x_t)\|^2 \sim \frac{\eta^2}{2}\nabla f_B(x_t)^\top \mathbf{A}_B\nabla f_B(x_t), \quad (2)$$

preventing the single-batch loss from diverging. This makes sense, as the gradient step is on the mini-batch loss, thus the training is stuck in an oscillatory regime when the single batch loss oscillates (on average)¹.

One might expect this to imply $\lambda_{\max}(\mathcal{H}(L_B)) \leq 2/\eta$, as in full-batch (1), but that is typically not the case. What is inducing (1) to rely on λ_{\max} is that the Hessians at every step share the eigenvectors relative to the highest eigenvalue. In mini-batch SGD, the sampled Hessians \mathbf{A}_B generally have completely different eigenspaces than \mathbf{A} and between each others. Indeed, the case of mini-batch SGD, we are working with the following quadratic Taylor approximation:

$$f_B(x) = \frac{1}{b} \sum_{i \in B} \left(\frac{1}{2} x^\top \mathbf{A}_i x + \mathbf{b}_i^\top x + \mathbf{c}_i \right), \quad (3)$$

where $B \subset \{1, 2, \dots, n\}$ is a randomly sampled mini batch of size b , and \mathbf{A}_i , \mathbf{b}_i , and \mathbf{c}_i represent coefficients on the quadratic losses of individual data points. Here the full-batch Hessian \mathbf{A} is given by $\mathbf{A} = \frac{1}{n} \sum_{i=1}^n \mathbf{A}_i$. Even if $\lambda_{\max}(\mathbf{A}) > 2/\eta$ with eigenvector v_{\max} , certain \mathbf{A}_i may map v_{\max} to 0 or a completely different vector, avoiding the blow-up seen in the full-batch regime.

Enforcing (2) in this setting (with $\mathbf{b}_i = 0$) thus results in

$$\frac{2}{\eta} \geq \sup_{v \in \mathbb{S}^d} \frac{v^\top \mathbb{E}_i [(\mathbf{A}_i)^3] v}{v^\top \mathbb{E}_i [(\mathbf{A}_i)^2] v} \stackrel{\text{which does not simplify to}}{\lambda_{\max}(\mathbf{A})}. \quad (4)$$

4.3. Why Stability cannot Depend on Full-Batch

We show here with an example that in the mini-batch setting the stability thresholds can not depend only on full-batch Hessian or gradients, but it *has to depend* on the higher moments of them over batch sampling, as we can always construct a counterexample which diverges otherwise.

Imagine on two data points we have $\mathbf{A}_1 = \alpha \cdot I + M$ and $\mathbf{A}_2 = \alpha \cdot I - M$, with $\alpha, \gamma > 0$ and $M = \begin{pmatrix} 0 & 0 \\ 0 & \gamma \end{pmatrix}$, and $\mathbf{b}_1 = \mathbf{b}_2 = 0$. Here \mathbf{A} is αI . \mathbf{A}_1 has eigenvalues $\alpha, \alpha + \gamma$ and \mathbf{A}_2 has eigenvalues $\alpha, \alpha - \gamma$.

Let us now look at possible full-batch stability results, as developed by Cohen et al. (2021). If the right stability notion for mini-batch SGD depended on the full-batch Hessian or gradients, then it would be independent on γ , and this can not be the case. For instance, if a notion as the one in Equation (1) would explain stability, then α could grow until $\alpha = 2/\eta$. However, *no matter the size of α* , if $\gamma > \max\{\alpha, \frac{2}{\eta} - \alpha\}$ a mini-batch iteration $x_{t+1} = (1 - \eta \mathbf{A}_i) x_t$ increases the size of the second component of x by a multiplicative factor bigger than 1.

¹After completion of this manuscript we found Lee & Jang (2023). We compare this with their work in Appendix C.

Thus a study of the stability of the system can not depend on the full-batch Hessian but has to depend on how big the oscillations due to the size of γ are, i.e., on the higher moments of the distribution of the mini-batch Hessian. Note that this situation would be even more extreme if we had (as in the practice of deep learning) the top eigenvectors of the mini-batch Hessians to point in completely different directions, not just to have high variance. As a sanity check, any stability threshold dependent on the higher moments of the mini-batch Hessian or gradients—as *Batch Sharpness* or $\mathbb{E}_B[\lambda_{\max}(\mathcal{H}(L_B))]$ —would induce η_{\max} to depend on γ too.

5. The Geometry of the Landscape at EOSS

We devote this section to the discussion of the sizes during training of different quantities which may be of interest of practitioners or theoreticians, as the λ_{\max} of full-batch and mini-batch Hessians in terms of learning rate, batch size, and critical batch size. For a batch size b , denote by

$$\lambda_{\max}^b := \mathbb{E}_{B \sim \mathcal{P}_b} [\lambda_{\max}(\mathcal{H}(L_B))].$$

Then, we establish here that:

- Also λ_{\max}^b stabilizes.
- λ_{\max}^b stabilizes at a level that ranges between $4/\eta$ and $2/\eta$. The level is lower for very small and very large batch sizes.
- λ_{\max}^b is always greater than λ_{\max} .
- We find that the level at which λ_{\max}^b stabilizes is characterized by two different regimes. The threshold is what we call *critical batch size*. This critical batch size depends on the complexity of the data-model.
- However, the gap between λ_{\max}^b and λ_{\max} typically goes as $1/b^\alpha$ generally with $\alpha = 0.70$. This is surprising, as when fixing the network, the gap goes as $1/b$ or $1/b^{1/2}$ both empirically and mathematically.

5.1. Average λ_{\max}^b for the mini-batch Hessians

We establish that λ_{\max}^b —the average over the possible batches sampled of the highest eigenvalue of the mini-batch Hessian—generally stabilizes at a value just bigger than $2/\eta$. This happens on a wide range of models and datasets.

We observe that its stabilization levels is generally very close to $2/\eta$ for very small batch sizes, it increases until the critical batch size, then it decreases again.

Interestingly, we observe that λ_{\max}^b responds to the change of parameters exactly as Cohen et al. (2021) observed for λ_{\max} in the full-batch setting.

5.2. Size of λ_{\max}

Although we show that the quantity of interest is the mini-batch Hessian, in case of mini-batch SGD, there are both historical and generalization-related reasons to investigate what the spectrum of the full-batch Hessian is.

We establish that also λ_{\max} generally stabilizes in the EOSS at a level which is strictly smaller than $2/\eta$. We show that the exact level at which λ_{\max} does not only depend on learning rate and batch size but on the full trajectory taken, unlike for EOS (Cohen et al., 2021). Indeed, in Section 3.3 we showed that it does not fully adapt to changes in hyper parameters. However, we observed that when we do not induce any shock in the system by changing hyper parameters during training, we can characterize two regimes for the stabilization levels, see Figure 6. Precisely

- (i) $b \leq \text{critical batch size}$: λ_{\max} grows with b with a power law.
- (ii) $b \geq \text{critical batch size}$: λ_{\max} grows with b much slower while approaching $2/\eta$ from below.

Unfortunately, we could not find a way to relate the size of λ_{\max} to learning rate and batch size—see Figure 9—if not through the gap it has with the average λ_{\max} of the mini-batch Hessian λ_{\max}^b . Notably, the *critical batch size* we mention is the point beyond which training enters the full-batch regime. Works as Zhang et al. (2024) study the following notion of *critical batch size*: "the point beyond which increasing batch size may result in computational efficiency degradation". We conjecture there may be a relation between the two quantities and we leave it to future work.

5.3. The Gap Between λ_{\max} and λ_{\max}^b

Note that conceptually λ_{\max}^b is inherently of the same nature as λ_{\max} , with the only difference being the "part" of the loss it is computed on—the mini-batch loss for the former, and full-batch loss for the latter. Yet, this difference proves to be crucial in being descriptive of the SGD training dynamics. Indeed, e.g.:

While the mini-batch gradients are an **unbiased** estimator of the full-batch gradient, $\lambda_{\max}(\mathcal{H}(L_B))$ is a **positively biased** estimator of λ_{\max} .

We indeed show in Lemma 4, that λ_{\max}^b is strictly bigger than λ_{\max} and, as a consequence, decreasing the batch size the gap increases. In particular,

$$\lambda_{\max}^1 < \lambda_{\max}^4 < \lambda_{\max}^{16} < \lambda_{\max}^{64} < \lambda_{\max}^{256} < \dots \quad (5)$$

We now empirically show what the gaps $\lambda_{\max}^b - \lambda_{\max}$ are, and we discuss why that is surprising. As shown in Appendix G and Figure 9, the log-log plot of the gap against batch size reveals three distinct regimes:

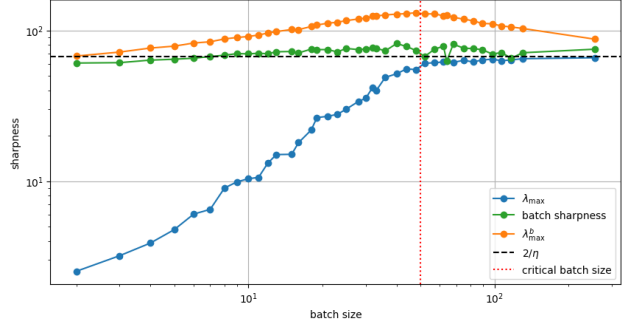


Figure 6. **Batch Sharpness vs. λ_{\max}^b vs. λ_{\max} at EOSS.** The values of *Batch Sharpness* (green), mini-batch λ_{\max}^b (orange), and full-batch λ_{\max} (blue) against varying batch sizes.

- **Very small b** : for extremely small batch sizes, the gap plateaus. This is unsurprising, as we are in the (i) regime for λ_{\max} .
- **Typical/moderate b** : the gap consistently scales as $1/b^{0.7}$ in the experiment. This trend dominates for a wide range of practical batch sizes, highlighting the systematic scaling behavior of the $\lambda_{\max}^b - \lambda_{\max}$ gap. It is important to note that we establish in Appendix G the exponent to be 0.7 independently from the depth, the seeds, the subsets of Cifar10 considered, and the architecture (MLP, CNN, ResNets). Also note that the *critical batch size* falls within this range. The limitation of this observation in describing λ_{\max} is that this consistent trend is consequence both of λ_{\max} growing and λ_{\max}^b decreasing, not just one of the two.
- **Very big b** : here generally λ_{\max}^b is essentially λ_{\max} and the gap is converging to zero, we conjecture that some form of scaling limit from random matrix theory applies here. The scaling law is generally of the form: $1/b^\alpha$ with $\alpha \geq 1$. The exact value of α may vary with the setting, but the overall trend is robust.

While the behavior for very small batches is not surprising, for bigger batch sizes it is. In computer vision tasks where there are way more parameters than datapoints, we observe that the *gap between λ_{\max}^b and λ_{\max} decreases linearly with $1/b$ when evaluating the λ_{\max}^b of any fixed model with different batch sizes, see Figure 8. This $1/b$ scaling is also what one expects from the analysis in Appendix F.*

6. Implications: Why Noise-Injected GD Differs from Mini-Batch SGD

6.1. SGD vs. Noisy Gradient Descent

A common belief is that SGD’s regularization stems from its “noisy” gradients, which find flatter minima. However, our analysis points to the *directional* structure of mini-batch noise as crucial. To test this, we compare mini-batch SGD

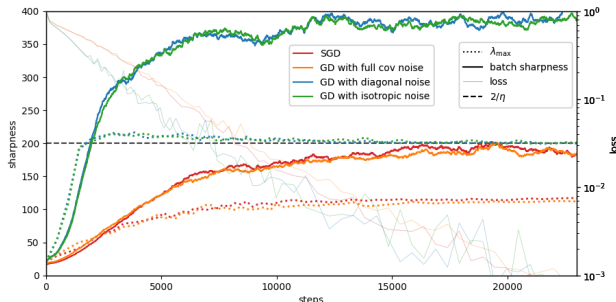


Figure 7. **SGD vs. Noisy GD.** Only noise preserving the covariance structure and direction of SGD leads to λ_{\max} plateauing below $2/\eta$ (akin to EOSS). Diagonal or isotropic noise fails to reproduce this behavior. Note that batch sharpness is still plotted for comparison, though for noisy GD it loses its meaning.

(batch size 16) against three noisy GD variants:

- *Directional Noise:* Gaussian noise matching the *directions and signs* of mini-batch SGD noise (Simsekli et al., 2019).
- *Diagonal Noise:* Gaussian noise restricted to the diagonal part of the SGD noise covariance.
- *Isotropic Noise:* Gaussian noise with isotropic covariance.

As shown in Fig. 7, only *directionally accurate* noise leads to an EOSS-like regime with λ_{\max} stabilizing well below $2/\eta$. More generic (diagonal or isotropic) noise fails to reproduce this behavior, indicating that standard SDE approximations—which typically ignore directional correlations—cannot fully capture the observed dynamics.

From a theoretical perspective (Appendix D), these experiments suggest that stability thresholds differ fundamentally between mini-batch SGD (governed by *Batch Sharpness*) and noise-injected GD (governed by λ_{\max}).

6.2. The Mini-Batch Landscape Matters

Classical analyses of neural network optimization often assume a single, static landscape: (i) **Online** perspective, modeling each sample’s gradient as a noisy unbiased estimator of the expected risk, or (ii) **Offline** perspective, treating the dataset as fixed and SGD as noisy GD on the empirical loss. In both views, it is the *full-batch* Hessian that supposedly drives curvature. Our results instead highlight the *mini-batch landscape*: each update sees a Hessian $\mathcal{H}(L_B)$ that can differ significantly from $\mathcal{H}(L)$, leading to *Batch Sharpness* stabilizing at $2/\eta$ even when full-batch λ_{\max} is much smaller.

6.3. Challenges for SDE Modeling

Prior works already note limitations of SDE-based approaches for SGD implicit regularization: they may be mathematically ill-posed (Yaida, 2018), fail except under

restrictive conditions (Li et al., 2021), converge to qualitatively different minima (HaoChen et al., 2020), or miss higher-order effects (Damian et al., 2021; Li et al., 2022). Recent discrete analyses (Roberts, 2021; Smith et al., 2021; Beneventano, 2023) attempt to address some of these issues. Nonetheless, our findings expose a deeper gap: when batch sizes are small, the *geometry of the mini-batch Hessian* differs markedly from that of the full-batch, altering both eigenvalues and eigenvector alignments. Conventional SDE models, which assume a static or average Hessian, cannot easily capture these rapid fluctuations. Fully accounting for the distribution of $\{\mathbf{A}_i\}$ remains an open challenge, emphasizing the need for further research into truly *batch-specific* dynamics.

7. Conclusions, Limitations, and Future Work

Conclusions. We introduced *Batch Sharpness* as a key descriptor of mini-batch SGD dynamics, showing that it stabilizes near $2/\eta$. This defines an *Edge of Stochastic Stability*, analogous to the classic EOS (Xing et al., 2018; Cohen et al., 2021; 2022), but now in the small-batch regime most commonly used in practice. Empirically, *Batch Sharpness* remains at $2/\eta$ while the full-batch λ_{\max} hovers below, at a level that systematically depends on batch size; indeed, the gap $\lambda_{\max}^b - \lambda_{\max}$ follows a power law (batch size) $^{-0.7}$ across various models and datasets.

Limitations. (i) We have tested only image-classification tasks, leaving open whether similar phenomena arise in NLP, RL, or other domains. (ii) Although we observe empirical batch-size scaling laws, we lack a full theoretical account, especially at moderate batch sizes. (iii) Our experiments mainly use fixed learning rates and standard architectures, so very large-scale or large-batch settings remain less explored. (iv) We have not analyzed momentum-based or adaptive methods (e.g. Adam), even though full-batch EOS has been seen there (Cohen et al., 2022).

Future Work. Beyond addressing these limitations, several directions remain: (i) Extending higher-order analyses (Damian et al., 2023; Cohen et al., 2021; Ahn et al., 2022; Lyu et al., 2023) to mini-batch SGD may clarify why *Batch Sharpness* $\sim 2/\eta$, (ii) Refining our batch-size scaling argument via random matrix theory might explain the “typical” exponent (around 0.7) and its possible crossovers for very large or very small batches.

In summary, *Batch Sharpness* provides a more faithful perspective on SGD than the full-batch λ_{\max} . Our findings highlight how mini-batch Hessians drive training instabilities and ultimately shape learned solutions, hopefully inspiring further research on how step size and batch size jointly govern deep network training.

Acknowledgement

A special thanks to Stanisław Jastrzębski, Alex Damian, Jeremy Cohen, Afonso Bandeira, Boris Hanin, Mark Lowell, and Renée Carmona for invaluable discussions, which were crucial to the development of this project. We acknowledge the use of DeepSeek, Claude, and ChatGPT for providing code assistance, debugging support, and editing suggestions.

Impact Statement

This paper presents work whose goal is to advance the field of Machine Learning. There are many potential societal consequences of our work, none which we feel must be specifically highlighted here.

References

- Achille, A., Rovere, M., and Soatto, S. Critical Learning Periods in Deep Neural Networks, 2017. URL <https://arxiv.org/abs/1711.08856v3>.
- Ahn, K., Zhang, J., and Sra, S. Understanding the unstable convergence of gradient descent. In *Proceedings of the 39th International Conference on Machine Learning*, June 2022. URL <https://proceedings.mlr.press/v162/ahn22a.html>.
- Ahn, K., Bubeck, S., Chewi, S., Lee, Y. T., Suarez, F., and Zhang, Y. Learning threshold neurons via the "edge of stability", October 2023. URL <http://arxiv.org/abs/2212.07469>. arXiv:2212.07469 [cs, math].
- Arora, S., Li, Z., and Panigrahi, A. Understanding Gradient Descent on Edge of Stability in Deep Learning, October 2022. URL <http://arxiv.org/abs/2205.09745>. arXiv:2205.09745 [cs].
- Beneventano, P. On the Trajectories of SGD Without Replacement, December 2023. URL <http://arxiv.org/abs/2312.16143>. arXiv:2312.16143.
- Beneventano, P. and Woodworth, B. Gradient Descent Converges Linearly to Flatter Minima than Gradient Flow in Shallow Linear Networks, January 2025. URL <http://arxiv.org/abs/2501.09137>. arXiv:2501.09137 [cs].
- Cohen, J. M., Kaur, S., Li, Y., Kolter, J. Z., and Talwalkar, A. Gradient Descent on Neural Networks Typically Occurs at the Edge of Stability. *arXiv:2103.00065 [cs, stat]*, June 2021. URL <http://arxiv.org/abs/2103.00065>. arXiv: 2103.00065.
- Cohen, J. M., Ghorbani, B., Krishnan, S., Agarwal, N., Medapati, S., Badura, M., Suo, D., Cardoze, D., Nado, Z., Dahl, G. E., and Gilmer, J. Adaptive Gradient Methods at the Edge of Stability, July 2022. URL <http://arxiv.org/abs/2207.14484>. arXiv:2207.14484 [cs].
- Cohen, J. M., Damian, A., Talwalkar, A., Kolter, Z., and Lee, J. D. Understanding Optimization in Deep Learning with Central Flows, October 2024. URL <http://arxiv.org/abs/2410.24206>. arXiv:2410.24206.
- Damian, A., Ma, T., and Lee, J. Label Noise SGD Provably Prefers Flat Global Minimizers. *arXiv:2106.06530 [cs, math, stat]*, June 2021. URL <http://arxiv.org/abs/2106.06530>. arXiv: 2106.06530.
- Damian, A., Nichani, E., and Lee, J. D. Self-Stabilization: The Implicit Bias of Gradient Descent at the Edge of Stability, April 2023. URL <http://arxiv.org/abs/2209.15594>. arXiv:2209.15594 [cs, math, stat].
- Dinh, L., Pascanu, R., Bengio, S., and Bengio, Y. Sharp minima can generalize for deep nets. In *Proceedings of the 34th International Conference on Machine Learning-Volume 70*, pp. 1019–1028. JMLR. org, 2017.
- Foret, P., Kleiner, A., Mobahi, H., and Neyshabur, B. Sharpness-Aware Minimization for Efficiently Improving Generalization, April 2021. URL <http://arxiv.org/abs/2010.01412>. arXiv:2010.01412 [cs, stat].
- Fort, S. and Ganguli, S. Emergent properties of the local geometry of neural loss landscapes, 2019. URL <https://arxiv.org/abs/1910.05929v1>.
- Fort, S. and Scherlis, A. The Goldilocks Zone: Towards Better Understanding of Neural Network Loss Landscapes. *Proceedings of the AAAI Conference on Artificial Intelligence*, 33(01):3574–3581, July 2019. ISSN 2374-3468. doi: 10.1609/aaai.v33i01.33013574. URL <https://ojs.aaai.org/index.php/AAAI/article/view/4237>. Number: 01.
- Goodfellow, I., Bengio, Y., and Courville, A. *Deep learning*. MIT press, 2016.
- Goyal, P., Dollár, P., Girshick, R., Noordhuis, P., Wesolowski, L., Kyrola, A., Tulloch, A., Jia, Y., and He, K. Accurate, large minibatch sgd: Training imagenet in 1 hour. *arXiv preprint arXiv:1706.02677*, 2017.
- HaoChen, J. Z., Wei, C., Lee, J. D., and Ma, T. Shape Matters: Understanding the Implicit Bias of the Noise Covariance. *arXiv:2006.08680 [cs, stat]*, June 2020. URL <http://arxiv.org/abs/2006.08680>. arXiv: 2006.08680.
- Hochreiter, S. and Schmidhuber, J. SIMPLIFYING NEURAL NETS BY DISCOVERING FLAT MINIMA. In *Advances in Neural Information Processing Systems*, volume 7. MIT

- Press, 1994. URL <https://proceedings.neurips.cc/paper/1994/hash/01882513d5fa7c329e940dda99b12147-Abstract.html>.
- Hochreiter, S. and Schmidhuber, J. Flat minima. *Neural Computation*, 9(1):1–42, 1997. Publisher: MIT Press.
- Izmailov, P., Podoprikin, D., Garipov, T., Vetrov, D., and Wilson, A. G. Averaging Weights Leads to Wider Optima and Better Generalization, February 2019. URL <http://arxiv.org/abs/1803.05407>. arXiv:1803.05407 [cs, stat].
- Jastrzębski, S., Kenton, Z., Arpit, D., Ballas, N., Fischer, A., Bengio, Y., and Storkey, A. Three Factors Influencing Minima in SGD. *arXiv:1711.04623 [cs, stat]*, September 2018. URL <http://arxiv.org/abs/1711.04623>. arXiv: 1711.04623.
- Jastrzębski, S., Kenton, Z., Ballas, N., Fischer, A., Bengio, Y., and Storkey, A. On the Relation Between the Sharpest Directions of DNN Loss and the SGD Step Length, December 2019. URL <http://arxiv.org/abs/1807.05031>. arXiv:1807.05031 [stat].
- Jastrzębski, S., Szymczak, M., Fort, S., Arpit, D., Tabor, J., Cho, K., and Geras, K. The Break-Even Point on Optimization Trajectories of Deep Neural Networks. *arXiv:2002.09572 [cs, stat]*, February 2020. URL <http://arxiv.org/abs/2002.09572>. arXiv: 2002.09572.
- Jastrzębski, S., Arpit, D., Astrand, O., Kerg, G., Wang, H., Xiong, C., Socher, R., Cho, K., and Geras, K. Catastrophic Fisher Explosion: Early Phase Fisher Matrix Impacts Generalization. *arXiv:2012.14193 [cs, stat]*, June 2021. URL <http://arxiv.org/abs/2012.14193>. arXiv: 2012.14193.
- Jiang, Y., Neyshabur, B., Mobahi, H., Krishnan, D., and Bengio, S. Fantastic Generalization Measures and Where to Find Them. *arXiv:1912.02178 [cs, stat]*, December 2019. URL <http://arxiv.org/abs/1912.02178>. arXiv: 1912.02178.
- Keskar, N. S., Mudigere, D., Nocedal, J., Smelyanskiy, M., and Tang, P. T. P. On large-batch training for deep learning: Generalization gap and sharp minima. *arXiv preprint arXiv:1609.04836*, 2016.
- Kleinberg, R., Li, Y., and Yuan, Y. An Alternative View: When Does SGD Escape Local Minima?, August 2018. URL <http://arxiv.org/abs/1802.06175>. arXiv:1802.06175 [cs].
- LeCun, Y. A., Bottou, L., Orr, G. B., and Müller, K.-R. Efficient backprop. In *Neural networks: Tricks of the trade*, pp. 9–48. Springer, 2012.
- Lee, S. and Jang, C. A new characterization of the edge of stability based on a sharpness measure aware of batch gradient distribution. In *International Conference on Learning Representations*, 2023. URL <https://api.semanticscholar.org/CorpusID:259298833>.
- Lewkowycz, A., Bahri, Y., Dyer, E., Sohl-Dickstein, J., and Gur-Ari, G. The large learning rate phase of deep learning: the catapult mechanism. *arXiv:2003.02218 [cs, stat]*, March 2020. URL <http://arxiv.org/abs/2003.02218>. arXiv: 2003.02218.
- Li, Y., Wei, C., and Ma, T. Towards explaining the regularization effect of initial large learning rate in training neural networks. In *Advances in Neural Information Processing Systems*, pp. 11669–11680, 2019.
- Li, Z., Malladi, S., and Arora, S. On the Validity of Modeling SGD with Stochastic Differential Equations (SDEs). *arXiv:2102.12470 [cs, stat]*, June 2021. URL <http://arxiv.org/abs/2102.12470>. arXiv: 2102.12470.
- Li, Z., Wang, T., and Arora, S. What Happens after SGD Reaches Zero Loss? –A Mathematical Framework. *arXiv:2110.06914 [cs, stat]*, February 2022. URL <http://arxiv.org/abs/2110.06914>. arXiv: 2110.06914.
- Lyu, K., Li, Z., and Arora, S. Understanding the Generalization Benefit of Normalization Layers: Sharpness Reduction, January 2023. URL <http://arxiv.org/abs/2206.07085>. arXiv:2206.07085 [cs].
- Martens, J. New Insights and Perspectives on the Natural Gradient Method, 2020.
- Masters, D. and Luschi, C. Revisiting Small Batch Training for Deep Neural Networks, April 2018. URL <http://arxiv.org/abs/1804.07612>. arXiv:1804.07612.
- Mishchenko, K., Khaled, A., and Richtarik, P. Random Reshuffling: Simple Analysis with Vast Improvements. In *Advances in Neural Information Processing Systems*, volume 33, pp. 17309–17320. Curran Associates, Inc., 2020. URL <https://proceedings.neurips.cc/paper/2020/hash/c8cc6e90ccbff44c9cee23611711cdc4-Abstract.html>.
- Murata, N., Yoshizawa, S., and Amari, S. Network information criterion-determining the number of hidden units for an artificial neural network model. *IEEE Transactions on Neural Networks*, 5(6):865–872, November 1994. ISSN 1941-0093. doi: 10.1109/72.329683. URL <https://ieeexplore.ieee.org/>

- [document/329683](#). Conference Name: IEEE Transactions on Neural Networks.
- Neyshabur, B., Bhojanapalli, S., Mcallester, D., and Srebro, N. Exploring Generalization in Deep Learning. In Guyon, I., Luxburg, U. V., Bengio, S., Wallach, H., Fergus, R., Vishwanathan, S., and Garnett, R. (eds.), *Advances in Neural Information Processing Systems 30*, pp. 5947–5956. Curran Associates, Inc., 2017. URL <http://papers.nips.cc/paper/7176-exploring-generalization-in-deep-learning.pdf>.
- Robbins, H. and Monro, S. A stochastic approximation method. *The annals of mathematical statistics*, pp. 400–407, 1951.
- Roberts, D. A. SGD Implicitly Regularizes Generalization Error. *arXiv:2104.04874 [cs, stat]*, April 2021. URL <http://arxiv.org/abs/2104.04874>. arXiv: 2104.04874.
- Sagun, L., Bottou, L., and LeCun, Y. Eigenvalues of the Hessian in Deep Learning: Singularity and Beyond, November 2016. URL <https://openreview.net/forum?id=B186cP9gx>.
- Simsekli, U., Sagun, L., and Gürbüzbalaban, M. A tail-index analysis of stochastic gradient noise in deep neural networks. *CoRR*, abs/1901.06053, 2019. URL <http://arxiv.org/abs/1901.06053>.
- Smith, S. L., Dherin, B., Barrett, D. G. T., and De, S. On the Origin of Implicit Regularization in Stochastic Gradient Descent. *arXiv:2101.12176 [cs, stat]*, January 2021. URL <http://arxiv.org/abs/2101.12176>. arXiv: 2101.12176.
- Thomas, V., Pedregosa, F., Merriënboer, B., Manzagol, P.-A., Bengio, Y., and Roux, N. L. On the interplay between noise and curvature and its effect on optimization and generalization. In *Proceedings of the Twenty Third International Conference on Artificial Intelligence and Statistics*, pp. 3503–3513. PMLR, June 2020. URL <https://proceedings.mlr.press/v108/thomas20a.html>. ISSN: 2640-3498.
- Wang, Y., Chen, M., Zhao, T., and Tao, M. Large learning rate tames homogeneity: Convergence and balancing effect. In *International Conference on Learning Representations*, 2022. URL <https://openreview.net/forum?id=3tbDrs77LJ5>.
- Wu, L., Zhu, Z., and E, W. Towards Understanding Generalization of Deep Learning: Perspective of Loss Landscapes. *arXiv:1706.10239 [cs, stat]*, November 2017. URL <http://arxiv.org/abs/1706.10239>. arXiv: 1706.10239.
- Xie, Z., Sato, I., and Sugiyama, M. A Diffusion Theory For Deep Learning Dynamics: Stochastic Gradient Descent Exponentially Favors Flat Minima. *arXiv:2002.03495 [cs, stat]*, November 2020. URL <http://arxiv.org/abs/2002.03495>. arXiv: 2002.03495.
- Xing, C., Arpit, D., Tsirigotis, C., and Bengio, Y. A Walk with SGD, May 2018. URL <http://arxiv.org/abs/1802.08770>. arXiv:1802.08770 [cs, stat].
- Yaida, S. Fluctuation-dissipation relations for stochastic gradient descent. *arXiv preprint arXiv:1810.00004*, 2018.
- Zhang, H., Morwani, D., Vyas, N., Wu, J., Zou, D., Ghai, U., Foster, D., and Kakade, S. How Does Critical Batch Size Scale in Pre-training?, November 2024. URL <http://arxiv.org/abs/2410.21676>. arXiv:2410.21676 [cs].
- Zhu, L., Liu, C., Radhakrishnan, A., and Belkin, M. Quadratic models for understanding catapult dynamics of neural networks, May 2024. URL <http://arxiv.org/abs/2205.11787>. arXiv:2205.11787 [cs].
- Zhu, X., Wang, Z., Wang, X., Zhou, M., and Ge, R. UNDERSTANDING EDGE-OF-STABILITY TRAINING DYNAMICS WITH A MINIMALIST EXAMPLE, 2023.

Table of Contents

- **1. Introduction** 1
- **2. Related Work** 2
- **3. SGD Typically Occurs at the EOSS** 3
- **4. Mathematics of Stability** 5
- **5. The Geometry of the Landscape at EOSS** 6
- **6. Implications: Why Noise-Injected GD Differs From Mini-Batch SGD** 7
- **7. Conclusions, Limitations, and Future Work** 8

- **A. On the Stability** 12
- **B. Stability for Mini-Batch SGD** 14
- **C. Comparison with Lee & Jang (2023)** 15
- **D. Stability for Noise-Injected Gradient Descents** 15
- **E. Sampling the Mini Batches** 16
- **F. On Largest Eigenvalues of Sums of Matrices** 17
- **G. Dependence of $\lambda_{\max}^b - \lambda_{\max}$ Gap on the Batch Size** 19
- **H. The Hessian and the Fisher Information Matrix Overlap** 21
- **I. Exemplification Through a Simplified Model** 24
- **J. Illustration of EOSS in Variety of Settings: λ_{\max}^b** 28
- **K. Illustration of EOSS in Variety of Settings: *Batch Sharpness*** 24

A. On the Stability

A.1. On Equivalent Formulations of Stability

Consider as working example the quadratic Taylor approximation of a loss function:

$$f(x) = \frac{1}{2}x^\top \mathbf{A}x + \mathbf{b}^\top x + \mathbf{c},$$

where \mathbf{A} is the Hessian matrix (symmetric and positive semidefinite), \mathbf{b} is the gradient vector, and \mathbf{c} is a constant.

The question of stability is very nuanced, and we decided to define stability and η_{\max} as follows

Definition 2 (Stability). We say that the optimization algorithm \mathcal{A} on the objective f is stable if it does not diverge.

By Folklore, in the quadratic objective f above, enforcing stability is equivalent to choosing a step size smaller than η_{\max} as follows.

Definition 3 (Step size at the edge for an algorithm). Specify a discrete-time optimization algorithm of choice \mathcal{A} . We define "step size at the edge for \mathcal{A} " the maximum step size $\eta_{\max}(\mathcal{A}) > 0$ under which the dynamics do not diverge along the whole trajectory in the quadratic objective case, meaning there does not exist a t such that $|x_{t+1} - x^*| > |x_t - x^*|$. In case of a stochastic update, we define $\eta_{\max}(\mathcal{A})$ analogously, but in expectation.

This is a good definition in the quadratic setting above, no matter how we define divergence, indeed

Lemma 1. *Let $f(x)$ be quadratic, specify a discrete-time optimization algorithm of choice \mathcal{A} . Then $\eta_{\max}(\mathcal{A}) > 0$ is the maximum step size under which the dynamics does not diverge to infinity. Both in terms of $f(x_t)$ and in terms of $\|x_t - x^*\|$.*

And we have, analogously, stability in terms of non-increasing loss.

Lemma 2. *Let $f(x)$ be quadratic, specify a discrete-time optimization algorithm of choice \mathcal{A} . Then $\eta_{\max}(\mathcal{A}) > 0$ is the maximum step size under which there does not exist a t such that $f(x_{t+1}) > f(x_t)$.*

A.2. Specialization of the Setting to Mini-Batch SGD

In the case of mini-batch SGD, we are working, instead, with the following 2-order Taylor approximation:

$$f_B(x) = \frac{1}{b} \sum_{i \in B} \left(\frac{1}{2} x^\top \mathbf{A}_i x + \mathbf{b}_i^\top x + \mathbf{c}_i \right), \quad (6)$$

where $B \subset \{1, 2, \dots, n\}$ is a randomly sampled mini batch of size b , and \mathbf{A}_i , \mathbf{b}_i , and \mathbf{c}_i represent contributions from individual data points. The full objective matrices are instead given by:

$$\mathbf{A} = \frac{1}{n} \sum_{i=1}^n \mathbf{A}_i, \quad \mathbf{b} = \frac{1}{n} \sum_{i=1}^n \mathbf{b}_i.$$

Update rule for mini-batch SGD. Here, the mini-batch SGD update rule is:

$$x_{t+1} = x_t - \eta \nabla f_B(x_t),$$

where the gradient for mini batch B is:

$$\nabla f_B(x_t) = \frac{1}{b} \sum_{i \in B} (\mathbf{A}_i x_t + \mathbf{b}_i) = \left[\frac{1}{b} \sum_{i \in B} \mathbf{A}_i \right] (x_t - x^*) + \left(\frac{1}{b} \sum_{i \in B} \mathbf{A}_i x^* + \mathbf{b}_i \right). \quad (7)$$

Substituting this gradient, the update becomes:

$$x_{t+1} = x_t - \eta \left(\frac{1}{b} \sum_{i \in B} \mathbf{A}_i x_t + \frac{1}{b} \sum_{i \in B} \mathbf{b}_i \right).$$

To analyze stability, one generally focuses on the evolution of the error $x_t - x^*$, where $x^* = -\mathbf{A}^{-1}\mathbf{b}$ is the optimum. By adding and subtracting x^* , we obtain that error evolves as:

$$x_{t+1} - x^* = \left(I - \eta \frac{1}{b} \sum_{i \in B} \mathbf{A}_i \right) (x_t - x^*) - \eta \left(\sum_{i \in B} \mathbf{A}_i x^* + \frac{1}{b} \sum_{i \in B} \mathbf{b}_i \right).$$

We can notice here the first difference with the full-batch case:

1. The rest $\sum_{i \in B} \mathbf{A}_i x^* + \frac{1}{b} \sum_{i \in B} \mathbf{b}_i$ it is different than 0 and it is different than 0 even in expectation when sampling is not uniform and independent.
2. The multiplier $\frac{1}{b} \sum_{i \in B} \mathbf{A}_i$ is not \mathbf{A} .

Next note that if we work with an full-batch GD with noise injected with *unbiased and independent steps* in the fashion of [Robbins & Monro \(1951\)](#), their expectation evens these terms out. We refer the reader to [Appendix D](#) for that. If we work with a *biased* algorithm, as Random Reshuffling (or SGD without replacement) or Shuffle Once, this is not the case ([Mishchenko et al., 2020](#); [Smith et al., 2021](#); [Beneventano, 2023](#)). We refer the reader to [Appendix E](#) for what changes in this setting.

Furthermore, while in the deterministic case working with $x_{t+1} - x^*$ or with $\|x_{t+1} - x^*\|^2$ is the same, this is not the case for mini-batch algorithms. It is thus non-obvious how to generalize stability to start with. We will see in the next section how to do it.

A.3. Formulating Stability for Mini-Batch SGD

Unlike in the deterministic case, we have to be a little more careful with the formulation here. Let (λ_i, v_i) be the ordered eigenvalue-eigenvector pairs of \mathbf{A} . With a deterministic Hessian matrix \mathbf{A} we have that $x_{t+1} - x^*$ does not diverge if and only if the highest eigenvalue α_i such that $\langle x_{t+1} - x^*, v_i \rangle \neq 0$ is smaller than $2/\eta$, see [Cohen et al. \(2021\)](#). The idea is that

if a component $\langle x_{t+1} - x^*, v_i \rangle \neq 0$ exists, after k steps it gets multiplied by $(1 - \eta\alpha_i)^k$. This implies that the system will diverge if and only if $|1 - \eta\alpha_i| > 1$. When our step is a noise-injected GD similar stability phenomena happens, \mathbf{A} is not impacted by the noise, see Appendix D.

However, in the case of mini-batch SGD we have to be much more precise, and note that at every step, stability does not depend on \mathbf{A} , but on the " \mathbf{A} " of the mini batch. We have an important changes here:

We do not have persistence of a Hessian matrix " \mathbf{A} ". In particular, there is no persistence in the eigenspaces of the Hessian from step to step. This implies that we can not make an argument as the one above tracking the components of $x_t - x^$. This will have an important implication, that at the step t we care about the direction we are moving towards, not about the eigenvector of the highest eigenvalue. We are now dealing with objects of the form $\nabla f^\top \cdot \nabla^2 f \cdot \nabla f$, not of the form $\lambda_{\max} \nabla^2 f$.*

This imply that we may not really work on the eigenspaces of \mathbf{A} as before, we decide to work with the analogous formulation of stability given by Lemma 2: For quadratic objectives, $|x_{t+1} - x^*| \leq |x_t - x^*|$ reduces in norm if and only if $f(x_{t+1}) \leq f(x_t)$. We will work from now on with the formulation of stability of $f(x_{t+1}) \leq f(x_t)$.

At the step t we can write the following thing update for a quadratic objective f .

$$f(x_{t+1}) - f(x_t) = -\eta \nabla f(x_t)^\top \nabla f(x_t) + \frac{\eta^2}{2} \nabla f(x_t)^\top \cdot \nabla^2 f(x_t) \nabla f(x_t) \leq 0 \quad (8)$$

which is equivalent to

$$2\|\nabla f(x_t)\| \geq \eta \nabla f(x_t)^\top \cdot \nabla^2 f(x_t) \cdot \nabla f(x_t). \quad (9)$$

Thus the stability of Cohen et al. (2021), from this perspective, is equivalent to enforcing for all t the inequality Equation (9), or analogously enforcing it in expectation.

Here, for full-batch GD we could argue that if $\langle x_t - x^*, v_1 \rangle$ and $\eta\lambda_1 > 2$ but $\eta\lambda_i < 2$ for all $i \in \{2, 3, \dots\}$ then there exists a time T , logarithmic in the initial values of x_0 , such that $f(x_{T+1}) > f(x_T)$. This time T is defined by the components 2+ being small enough and the first one big enough that the $|1 - \eta\lambda_1| > 1$ update on the first components outweigh the decrease in the others.

B. Stability for Mini-Batch SGD

In the case of mini-batch SGD we have an update on the mini-batch loss. To get to the loss from the mini-batch loss, we can just take an expectation over the batch-sampling process. Thus, by taking the expectation at every algorithm step we can write the stability requirement as

$$\mathbb{E}_{\text{batches}} [f_B(x_{t+1}) - f_B(x_t)] = -\eta \mathbb{E}_{\text{batches}} [\nabla f_B(x_t)^\top \nabla f_B(x_t)] + \frac{\eta^2}{2} \mathbb{E}_{\text{batches}} [\nabla f_B(x_t)^\top \nabla^2 f_B(x_t) \nabla f_B(x_t)] \leq 0. \quad (10)$$

This leads to our lemma

Lemma 3. $\mathbb{E}[f_B(x_{t+1})] \leq \mathbb{E}[f_B(x_t)]$ if and only if the step size η is smaller than 2 divided by

$$\text{Batch Sharpness} = \frac{\mathbb{E}_{\text{batches}} [\nabla f_B(x_t)^\top \cdot \nabla^2 f_B(x_t) \cdot \nabla f_B(x_t)]}{\mathbb{E}_{\text{batches}} [\|\nabla f_B(x_t)\|^2]}.$$

Proof. Note that the Taylor expansion as in Equation 10 ensures that

$$\mathbb{E}[f_B(x_{t+1})] \leq \mathbb{E}[f_B(x_t)] = \mathbb{E} \left[-\eta \nabla f_B(x_t)^\top \nabla f_B(x_t) + \frac{\eta^2}{2} \nabla f_B(x_t)^\top \cdot \nabla^2 f_B(x_t) \nabla f_B(x_t) \right]$$

Thus, by enforcing $\mathbb{E}[f_B(x_{t+1})] \leq \mathbb{E}[f_B(x_t)]$ is equivalent to enforcing

$$2 \geq \eta \cdot \text{Batch Sharpness}.$$

Taking this expectation over the ways in which we can sample the batches we conclude the proof. \square

C. Comparison with Lee & Jang (2023)

After we wrote the first version of this article, we realized that Lee & Jang (2023) already dealt with this problem. We draw here a comparison and show that they come to a different conclusion because they deal with a different notion of stability. While our batch sharpness and their Interaction-Aware Sharpness (IAS) are similar in the experiments—and about the same in case of bigger batch sizes, we discuss how our two notions of stability relate to the one of Cohen et al. (2021).

They propose that the quantity which stabilizes around $2/\eta$ is, in our notation,

$$\text{IAS} := \frac{\mathbb{E}_{\text{batches}} [\nabla f_B^\top \cdot \nabla^2 f \cdot \nabla f_B]}{\|\nabla f\|^2} = \frac{\text{tr} \left(\nabla^2 f \cdot \mathbb{E}_{\text{batches}} [\nabla f_B \nabla f_B^\top] \right)}{\text{tr} (\nabla f \nabla f^\top)}. \quad (11)$$

The very natural way they come up with this quantity is by imposing the following inequality, similar to our Equation (10).

$$\mathbb{E}_{\text{batches}} \left[\underbrace{f(x_{t+1}) - f(x_t)} \right] = -\eta \mathbb{E}_{\text{batches}} \left[\underbrace{\nabla f(x_t)^\top \nabla f_B(x_t)} \right] + \frac{\eta^2}{2} \mathbb{E}_{\text{batches}} \left[\underbrace{\nabla f_B(x_t)^\top \cdot \nabla^2 f(x_t) \nabla f_B(x_t)} \right] \leq 0. \quad (12)$$

The difference between our Equation (10) and this equation above is that the terms in which we put a under brace are here evaluated on the whole dataset and not on the mini batch considered.

While the inequalities seem analogous and both equally motivated at first glance, we claim they carry an important difference. Enforcing Equation (12) does imply that in 1 step the loss does not go up. However, it does not imply that the loss will not go up *eventually*. The instability threshold discussed in Cohen et al. (2021), in the following work, and in our is stability about the whole trajectory, not about one precise step of the optimizer in consideration.

As an example to show this, imagine we are in the easiest possible quadratic setting, as above. Assume that $\mathbb{E}_{\text{batches}} [\langle \nabla f_B, v_1(\mathbf{A}) \rangle^2] \neq 0$ and $\lambda_1(\mathbf{A}) > 2/\eta$ and that there exist other eigenvalues λ_d which are instead smaller than $\lambda_d \leq 2/\eta$. Then imposing $\text{IAS} \leq 2/\eta$ implies that in one step the loss decreases.

$$\begin{aligned} 2/\eta \geq \text{IAS} &= \frac{1}{\|\nabla f\|^2} (\nabla f^\top \cdot \nabla^2 f \cdot \nabla f \mathbb{E} [\zeta_B^\top \cdot \nabla^2 f \cdot \zeta_B]) \\ &= \frac{1}{\|\nabla f\|^2} \sum_{i=1}^d \lambda_i (\langle \nabla f, v_i \rangle^2 + \mathbb{E}[\langle \zeta_B, v_i \rangle^2]). \end{aligned} \quad (13)$$

However, after T steps we can lower bound the loss with an increasing sequence which eventually diverges. Moreover, the loss asymptotically will approach the sequence with a linear convergence rate. Precisely, define the noise ζ_B such that $\nabla f_B = \nabla f + \zeta_B$. Then, for instance, if ∇f of the noise ζ_B have scalar product different than 0 with v_d , enforcing Equation (12) of Lee & Jang (2023) we may have decrease in loss in one step, indeed

$$\begin{aligned} f(x_T) - f(x_0) &= \sum_{t=0}^{T-1} \left(\frac{\eta^2}{2} \sum_{i=1}^d \lambda_i (\langle \nabla f(x_t), v_i \rangle^2 + \mathbb{E}[\langle \zeta_B(x_t), v_i \rangle^2]) - \|\nabla f(x_t)\|^2 \right) \\ &\geq \underbrace{\sum_{t=0}^{T-1} \left(\frac{\eta^2}{2} \lambda_1 - \eta \right) \langle \nabla f(x_t), v_1 \rangle^2}_{\text{positive}} + \underbrace{\frac{\eta^2}{2} \mathbb{E}[\langle \zeta_B(x_t), v_1 \rangle^2]}_{\text{positive}}. \end{aligned} \quad (14)$$

Both the quantities under-braced above—the parallel component to v_1 —explode with the time t . This implies, in particular, that imposing $\text{IAS} \leq 2/\eta$ may implies one-step stability, but not trajectory stability.

Our quantity, in turn, factors in the variability that the eigenspaces have on different batches. Our quantity is also strictly bigger, thus imposing it to be equal to $2/\eta$ induces a lower sharpness, see, e.g. Appendices G and I.

D. Stability for Noise-Injected Gradients Descents

We will see here that what we showed above is the case of mini-batch algorithms but not of many other versions of stochastic algorithms considered in theoretical work or practice.

We deal here with the case of noisy gradients, which is the case usually analyzed in the practice of theory works, see Section 6. While in minibatch stochastic gradient descent (SGD), the step function is

$$x_{t+1} = x_t - \eta \left(\frac{1}{b} \sum_{i \in B} \mathbf{A}_i x_t + \frac{1}{b} \sum_{i \in B} \mathbf{b}_i \right).$$

and the noise comes from mini batching as shown above, in noisy gradient descents we do not care of a possible way to rewrite A, b, c as sum of other terms. Just, there exists a random variable ζ_t , independent for different times $t_1 \neq t_2$, such that the $t - th$ step is

$$x_{t+1} = x_t - \eta (\mathbf{A}(\mathbf{x}_t + \zeta_t) + b).$$

This implies that

$$x_{t+1} - x^* = (I + \eta \mathbf{A}) (x_t - x^*) + A \zeta_t.$$

This imply that the Hessian does not change from step to step. The expected stability formulation is actually the one of [Lee & Jang \(2023\)](#) in the sense of [Cohen et al. \(2021\)](#) is obtained for $\eta_{\max} = 2/\lambda_{\max}(\mathbf{A})$, as discussed above in Appendix C.

This, in particular, establishes mathematically and agrees with what we see empirically in Section 6.

E. Sampling the Mini Batches

For simplicity let us work with the one dimensional case. The point in this section is that In the one dimensional case where $\mathbf{A}_i = \mathbf{a}_i, \mathbf{b}_i, \mathbf{c}_i \in \mathbb{R}$ for all $i \in \{1, 2, \dots, n\}$ we have that

$$\mathbb{E}_{\text{sampling B}} [x_{t+1} - x^*] = \underbrace{\mathbb{E} \left[\left(1 - \eta \frac{1}{b} \sum_{i \in B} \mathbf{a}_i \right) (x_t - x^*) \right]}_{(1 - \eta \mathbf{a}) \cdot \mathbb{E}[x_{t+1} - x^*] \text{ when independent steps}} - \underbrace{\mathbb{E}_{\text{sampling B}} \left[\frac{1}{b} \sum_{i \in B} \mathbf{a}_i x^* + \frac{1}{b} \sum_{i \in B} \mathbf{b}_i \right]}_{0 \text{ when uniform sampling}}. \quad (15)$$

When a_i, b_i are sampled uniformly within the dataset and independently of the step t , then this becomes

$$\mathbb{E}_{\text{sampling B}} [x_{t+1} - x^*] = (1 - \eta \mathbf{a}) \mathbb{E}_{\text{sampling B}} [x_t - x^*] \quad (16)$$

and the stability threshold is the same as for full-batch GD or any other momentum version, for instance.

In SGD without replacement the "independent steps" are now the epochs, we thus work wlog with an epoch at once exactly in the fashion of [Beneventano \(2023\)](#) as the tools previously developed by [Mishchenko et al. \(2020\)](#); [Smith et al. \(2021\)](#) only work for infinitesimal step size and the tools in Appendix E of [Beneventano \(2023\)](#) are the only ones which allow us to consider more products *and* big learning rate. Let $k = n/b$ be the number of batches in an epoch and call B_j the batch of $j - th$ step and $\mathbf{a}_{B_j}, \mathbf{b}_{B_j}$ the averages of \mathbf{a} and \mathbf{b} over the batch B_j .

$$x_k - x^* = \prod_{j=1}^k (1 - \eta \mathbf{a}_{B_j}) (x_t - x^*) - \sum_{j=1}^k \left[\prod_{h=j+1}^k (1 - \eta \mathbf{a}_{B_h}) \right] (\mathbf{a}_{B_j} x^* + \mathbf{b}_{B_j}). \quad (17)$$

Next note that by taking the expectation of the term $\prod_{j=1}^k (1 - \eta \mathbf{a}_{B_j})$ we obtain

$$\mathbb{E} \left[\prod_{j=1}^k (1 - \eta \mathbf{a}_{B_j}) \right] = (1 - \eta \mathbf{a})^k + \frac{\eta^2}{n-1} \binom{k}{2} \left[\frac{1}{n} \sum_{i=1}^n a_i^2 - a^2 \right] + \dots$$

Here if $\eta = O\left(\frac{b^2}{n} [\text{Var}(\mathbf{a}_1)]^{-1}\right)$ which is generally very small, the second term may already be of size $O(1)$. We already see that in this case η of the instability threshold has to be set also through the variance of the \mathbf{a}_i , the size of the batch or the number of batches. More generally, by applying the results in Appendix E of [Beneventano \(2023\)](#) we obtain that

$$\mathbb{E} \left[\prod_{j=1}^k (1 - \eta \mathbf{a}_{B_j}) \right] = (1 - \eta \mathbf{a})^k - \kappa_k (1 - \eta \mathbf{a}_i) \quad (18)$$

and analogously

$$\mathbb{E} \left[\sum_{j=1}^k \left[\prod_{h=j+1}^k (1 + \eta \mathbf{a}_{B_h}) \right] (\mathbf{a}_{B_j} x^* + \mathbf{b}_{B_j}) \right] = - \sum_{j=1}^k \kappa_j (1 + \eta \mathbf{a}_k, 1 + \eta \mathbf{a}_{k-1}, \dots, 1 + \eta \mathbf{a}_{j+1}, \mathbf{a}_j x^* + \mathbf{b}_j) \quad (19)$$

where $\kappa_k(X)$ is the k -th cumulant of the random variable X , which here has an empirical distribution from which we sample the \mathbf{a}_i s.

This implies that the fact of sampling without replacement already implies different η for the edge of stability. We are now ready to deal with the main case.

F. On Largest Eigenvalues of Sums of Matrices

In this section we establish mathematically how the gap between *Batch Sharpness* and λ_{\max} scales with the batch size. Precisely, what size we can expect from the *Batch Sharpness*- λ_{\max} gap for fixed network.

In particular, the following linear algebra results collectively enhance our understanding of the stability and scaling properties of the largest eigenvalues in the context of matrix sums.

F.1. Ordering the Largest Eigenvalues.

The largest singular value of the Hessian matrix derived from single data points is positive. This observation is crucial in establishing the following well-known property of matrix eigenvalues.

Lemma 4. *Let $m, b \in \mathbb{N}$ and consider m matrices $M_1, M_2, \dots, M_b \in \mathbb{R}^{m \times m}$ satisfying $\lambda_{\max} > |\lambda_{\min}|$. Then, the largest eigenvalue of their sum satisfies*

$$\lambda_{\max} \left(\sum_{i=1}^b M_i \right) \leq \sum_{i=1}^b \lambda_{\max} (M_i) \quad (20)$$

with equality only if all M_i are identical.

This lemma is a direct consequence of the convexity of the operator norm in matrices and the fact that the largest eigenvalue is positive in our setting. In our setting, it implies that with non-identical matrices, the maximum eigenvalue of the sum is strictly less than the sum of the maximum eigenvalues of the individual matrices. To illustrate, consider eigenvalue sequences for batch sizes that are powers of four, though the result generalizes to any $b_1 < b_2$:

$$\lambda_{\max}^1 < \lambda_{\max}^4 < \lambda_{\max}^{16} < \lambda_{\max}^{64} < \lambda_{\max}^{256} < \dots \quad (21)$$

F.2. Trends of λ_{\max} given b

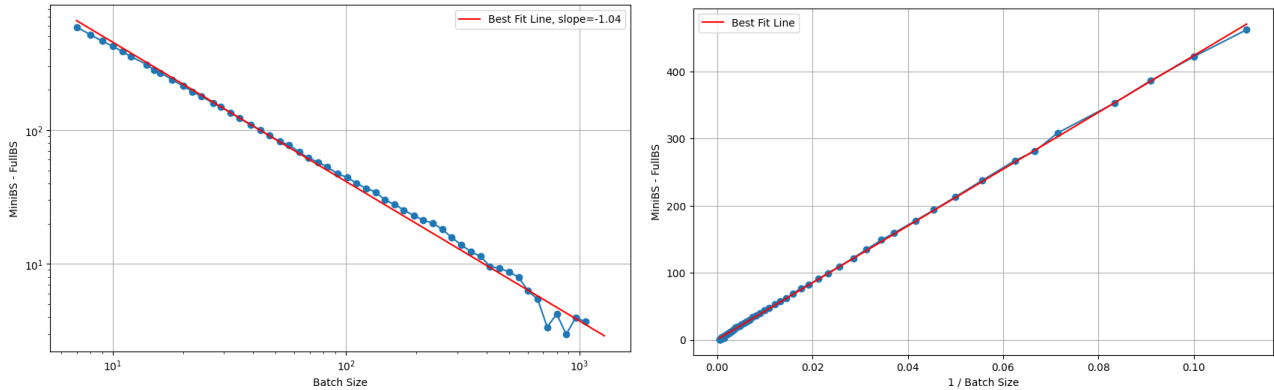


Figure 8. The *static* difference between λ_{\max}^b and λ_{\max} vs `batch_size`. The log-log plot is above, indicating the $1/\text{batch_size}$ dependence. The plot with $1/\text{batch_size}$ is below. We fix the parameters of the network at the end of training, and compute the λ_{\max}^b using the definition 1. This means that the λ_{\max} stays constant, and is subtracted for consistency.

As we discuss in Section 5.3, while the behavior we observe for very small batches is not surprising, for bigger batch sizes it is. In computer vision tasks where there are way more parameters than datapoints, we observe that the *gap between* λ_{\max}^b and λ_{\max} *decreases linearly with* $1/b$ when evaluating the λ_{\max}^b of any fixed model with different batch sizes, see Figure 8. This $1/b$ scaling is also what we expect from our mathematical analysis in Appendix F. We are indeed able to establish that for a fixed net, the gap scales as $1/b$ for small batch sizes, when the worst case λ_{\max}^b is very different from λ_{\max} , and with $1/\sqrt{b}$ for big batch sizes². Indeed:

Proposition 1 (Expected Size of the Average of Matrices). *In the notations of Lemma 4. Under the same assumptions as Lemma 5, the spectral norm of the deviation of the average $\|\frac{1}{b} \sum_i M_i - M\|$ from its expectation M satisfies:*

$$\left\| \frac{1}{b} \sum_i M_i - M \right\| = O_b \left(\sqrt{\frac{\sigma^2 \log m}{b}} + \frac{B \log m}{b} \right)$$

where $\sigma^2 = \frac{1}{b} \max\{\|\mathbb{E}[\sum_i M_i^\top M_i]\|, \|\mathbb{E}[\sum_i M_i M_i^\top]\|\}$ is the expected second moment of the matrices and $B \geq \|M_i - M\|$, for all i , is a bound to the biggest random matrix M_i .

F.3. Random Matrix Theory for Scaling Eigenvalues.

While Section 5 establishes mathematically the order of *Batch Sharpness*, it lacks of mathematical quantification of their magnitudes. Random matrix theory helps bridging this gap at least for big batch sizes b in the Online SGD case where instead of the full-batch Hessian we take as a reference its theoretical expectation.

Lemma 5 (Matrix Bernstein Inequality). *Let $n_1, n_2, b \in \mathbb{N}$, let $M_1, M_2, \dots, M_b \in \mathbb{R}^{n_1 \times n_2}$ be independent random matrices satisfying $\mathbb{E}[M_i] = M$ and $\|M_i - M\| \leq B$ for all i , let $v = \max\{\|\mathbb{E}[\sum_i M_i^\top M_i]\|, \|\mathbb{E}[\sum_i M_i M_i^\top]\|\}$ then for all $t > 0$*

$$\mathbb{P}(\|\sum_i M_i - M\| \geq t) \leq (n_1 + n_2) \cdot \exp\left(-\frac{b^2 t^2 / 2}{v + Bbt/3}\right).$$

This lemma provides a probabilistic upper bound on the deviation of the largest eigenvalue as the batch size increases. We now state a proposition that quantifies the expected spectral norm of the average of b matrices M_i based on this inequality.

Proof of 1. The Matrix Bernstein inequality bounds the probability of deviation of $|\sum_{i=1}^b (M_i - M)|$ by t . Rescaling by $1/b$, we see that for the average $\bar{M}_b := \frac{1}{b} \sum_{i=1}^b M_i$ we have

$$\mathbb{P}(\|\bar{M}_b - M\| \geq t/b) \leq (n_1 + n_2) \cdot \exp\left(-\frac{b^2 t^2 / 2}{v + Bbt/3}\right).$$

To bound the expectation $\mathbb{E}[\|\bar{M}_b - M\|]$, we use the following general inequality for random variables X with tail bounds:

$$\mathbb{E}[X] \leq \int_0^\infty \mathbb{P}(X \geq t) dt.$$

For $X = \|\bar{M}_b - M\|$, substitute the tail bound:

$$\mathbb{E}[\|\bar{M}_b - M\|] \leq \int_0^\infty (n_1 + n_2) \cdot \exp\left(-\frac{b^2 t^2 / 2}{v + Bbt/3}\right) dt.$$

We now, introduce a substitution to handle the exponential term. Let:

$$z = \frac{b^2 t^2}{v}, \quad \text{so that} \quad t = \sqrt{\frac{vz}{b^2}} \quad \text{and} \quad dt = \frac{1}{2} \sqrt{\frac{v}{b^2 z}} dz.$$

Rewriting the integral in terms of z :

$$\mathbb{E}[\|\bar{M}_b - M\|] \leq (n_1 + n_2) \int_0^\infty \exp\left(-\frac{z}{2 + \frac{Bb}{3\sqrt{vz}}}\right) \cdot \frac{1}{2} \sqrt{\frac{v}{b^2 z}} dz.$$

²Although big b means such that the number of directions spanned in the parameter space by the vectors $\nabla_\theta f(\theta, x)$ are repeated multiple times, and that may be practically unrealistic with the current sizes of networks.

While this integral is complex in its full form, we focus on the dominant terms by examining the asymptotics Large b :

- **Variance Contribution:** The v -term dominates when z is small. This leads to a contribution proportional to:

$$O\left(\frac{\sqrt{v \log(n_1 + n_2)}}{b}\right).$$

- **Max Norm Contribution:** The B -term dominates when z is large. This leads to a contribution proportional to:

$$O\left(\frac{B \log(n_1 + n_2)}{b}\right).$$

Combining these contributions gives:

$$\mathbb{E}[\|\bar{M}_b - M\|] = O\left(\frac{\sqrt{v \log(n_1 + n_2)}}{b} + \frac{B \log(n_1 + n_2)}{b}\right).$$

Next note that $v = b \cdot \sigma^2$. This concludes the proof of Proposition 1. □

The proposition indicates that as b increases, the expected deviation of \bar{M}_b from M diminishes, with a leading-order term scaling as:

1. **Variance Decay:** The term $\sqrt{\sigma^2/b}$ reflects how the variance contribution decreases as b increases (similar to $1/\sqrt{b}$ scaling for scalar averages).
2. **Norm Bound Decay:** The term B/b reflects how the worst-case individual matrix norm affects the average.
3. **Logarithmic Dimension Dependence:** The $\log(n_1 + n_2)$ factor accounts for the high-dimensional nature of the problem.

G. Dependence of $\lambda_{\max}^b - \lambda_{\max}$ Gap on the Batch Size

In this appendix, we further discuss the dependence of the gap between λ_{\max}^b and λ_{\max} from the batch size. As mentioned earlier, there are two distinct cases - the *static* case, and the "trained" case. In the former, we fix a model at some point of the training, and vary the batch size. In particular, λ_{\max} stays constant, and the only variation comes from λ_{\max}^b . In the latter, we fix a batch size at the beginning of the training, and look at the $\lambda_{\max}^b - \lambda_{\max}$ gap at the end of the training.

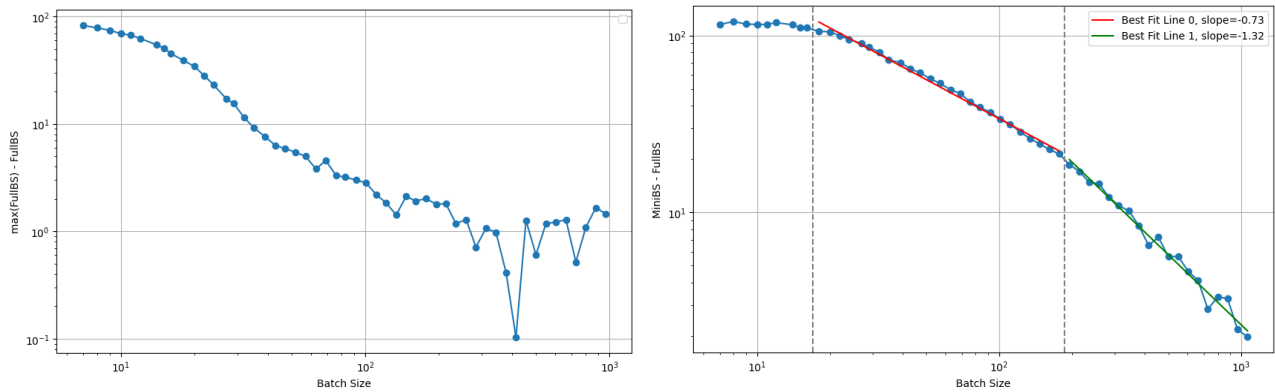


Figure 9. Log-log plots of (LHS) the gap between the maximum reached by the λ_{\max} and the λ_{\max} vs batch size; (RHS) $\lambda_{\max}^b - \lambda_{\max}$ gap vs batch size.

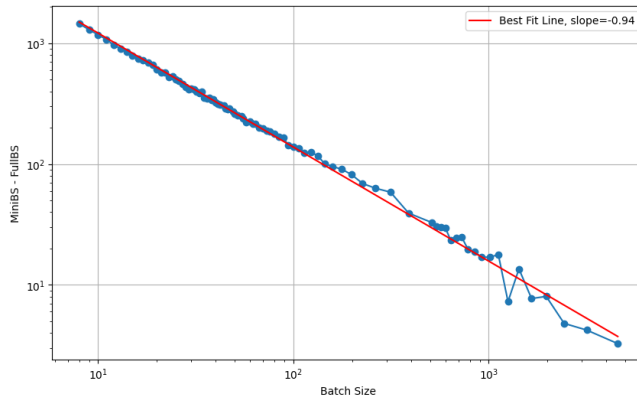


Figure 10. Log-log plot of the $\lambda_{\max}^b - \lambda_{\max}$ for fixed model at convergence.

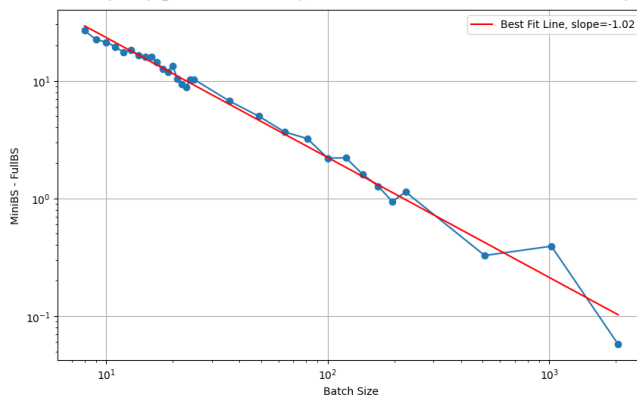


Figure 11. Log-log plot of the $\lambda_{\max}^b - \lambda_{\max}$ for a model at initialization

G.1. The static case

For the *static* case, we first look at a network at the end of training. The network is a preceptron with two hidden layers of dimension 512, trained with batch size of 256 on a 8k subset of CIFAR-10 to convergence. Log-log plot in Figure 10 confirms an approximate $1/\text{batch_size}$ dependence.

One can notice that at high batch sizes the observed slope is somewhat bigger (-1.1 if fitted to the $\lambda_{\max}^b - \lambda_{\max}$ computed for batch sizes larger than 1000). Now, for a dataset of size 8k, a batch size of 1000 constitutes $1/8$ of dataset, and thus has the λ_{\max}^b very close to the λ_{\max} . This might potentially reveal a different scaling regime for batch sizes that are closer to dataset size. On the other hand, since the difference between λ_{\max}^b and λ_{\max} becomes increasingly small when batch size approaches dataset size (especially in comparison to the value of each: $\lambda_{\max}^b - \lambda_{\max}$ being of order of 1, and each being around 500), the change in scaling might just be an effect of noise in estimating the highest eigenvalue of the hessian. Lastly, there is the effect of finiteness of the dataset size - that is, that the $1/b$ dependence would turn to 0 only when b is infinite, although in reality the gap would be 0 when b is equal to the dataset size. This dependence might effectively break the scaling. Answering the above questions necessitates further investigation. Nonetheless, the $1/b$ dependence appears to persist within the 'realistic' SGD regime, characterized by batch sizes that are substantially smaller than the dataset size.

The $1/b$ scaling appears to hold throughout the training. In particular, it also applies at initialization, as showcased in the log-log in Figure 11.

Moreover, the $1/b$ dependence is also architecture-independent. As illustrated in the log-log plot in Figure 12, it is also the case for a CNN architecture at convergence.

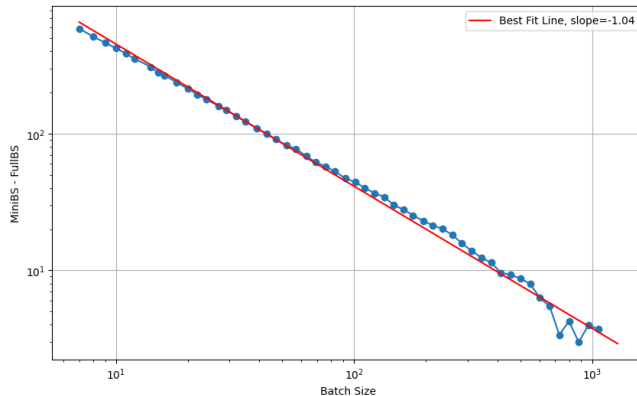


Figure 12. Log-log plot of the $\lambda_{\max}^b - \lambda_{\max}$ for fixed CNN model at convergence.

G.2. The trained case

As illustrated in Figure 13, the $1/\text{batch_size}$ dependence breaks down in the trained case, holding only within specific ranges of batch sizes. Specifically, for batch sizes in the range $[10, 100]$ the gap appears to scale as $1/b^{0.7}$. Meanwhile, for batch sizes in $[100, 1000]$, the gap scales as $1/b$. The corresponding regimes are depicted in Figure 14 and in Figure 15.

Similar to the static case, we again see that the anomalous region at batch sizes that are larger than $1/8$, requiring further investigation. A distinct scaling regime emerges for very small batch sizes (< 10), differing from the patterns described above. In this regime, the gap appears largely independent of the batch size. This anomaly might arise because, at such small batch sizes, the λ_{\max}^b starts at levels at or beyond the EOSS level, bypassing the standard progressive sharpening phase and instead entering a regime where the λ_{\max} decreases. Further investigation is necessary to rigorously characterize the scaling behavior in this regime.

H. The Hessian and the Fisher Information Matrix Overlap

We show here empirically that at EOSS generally λ_{\max}^b generally overlaps with the largest eigenvalue of the averaged mini-batch NTK and $\frac{1}{b} J_B^T J_B$, which corresponds with the FIM in vision classification tasks. See Figure 16.

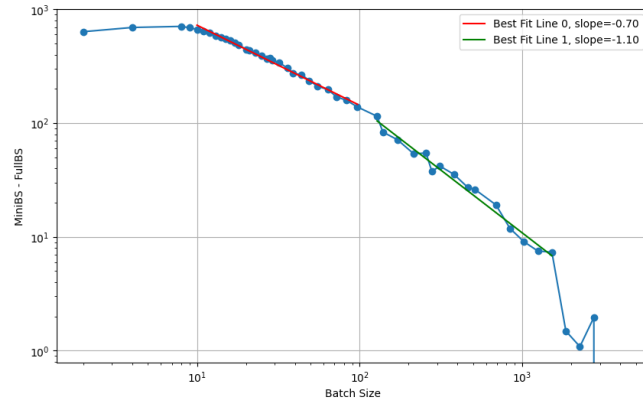


Figure 13. Log-log plot of $\lambda_{\max}^b - \lambda_{\max}$ gap vs batch size at the EOSS. Notice how the scaling breaks for very small and very large batch sizes

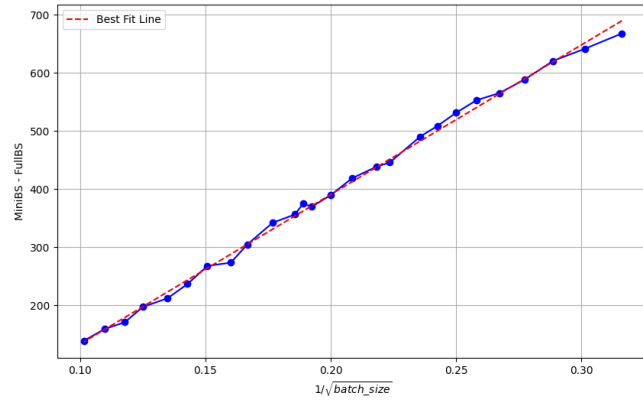


Figure 14. $\lambda_{\max}^b - \lambda_{\max}$ gap vs $1/\sqrt{\text{batch_size}}$ at the EOSS, for batch sizes in $[10, 100]$.

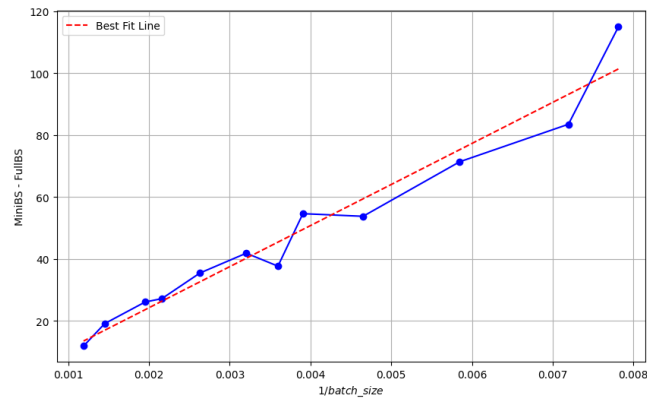


Figure 15. $\lambda_{\max}^b - \lambda_{\max}$ gap vs $1/\text{batch_size}$ at the EOSS, for batch sizes in $[100, 1000]$.

Edge of Stochastic Stability

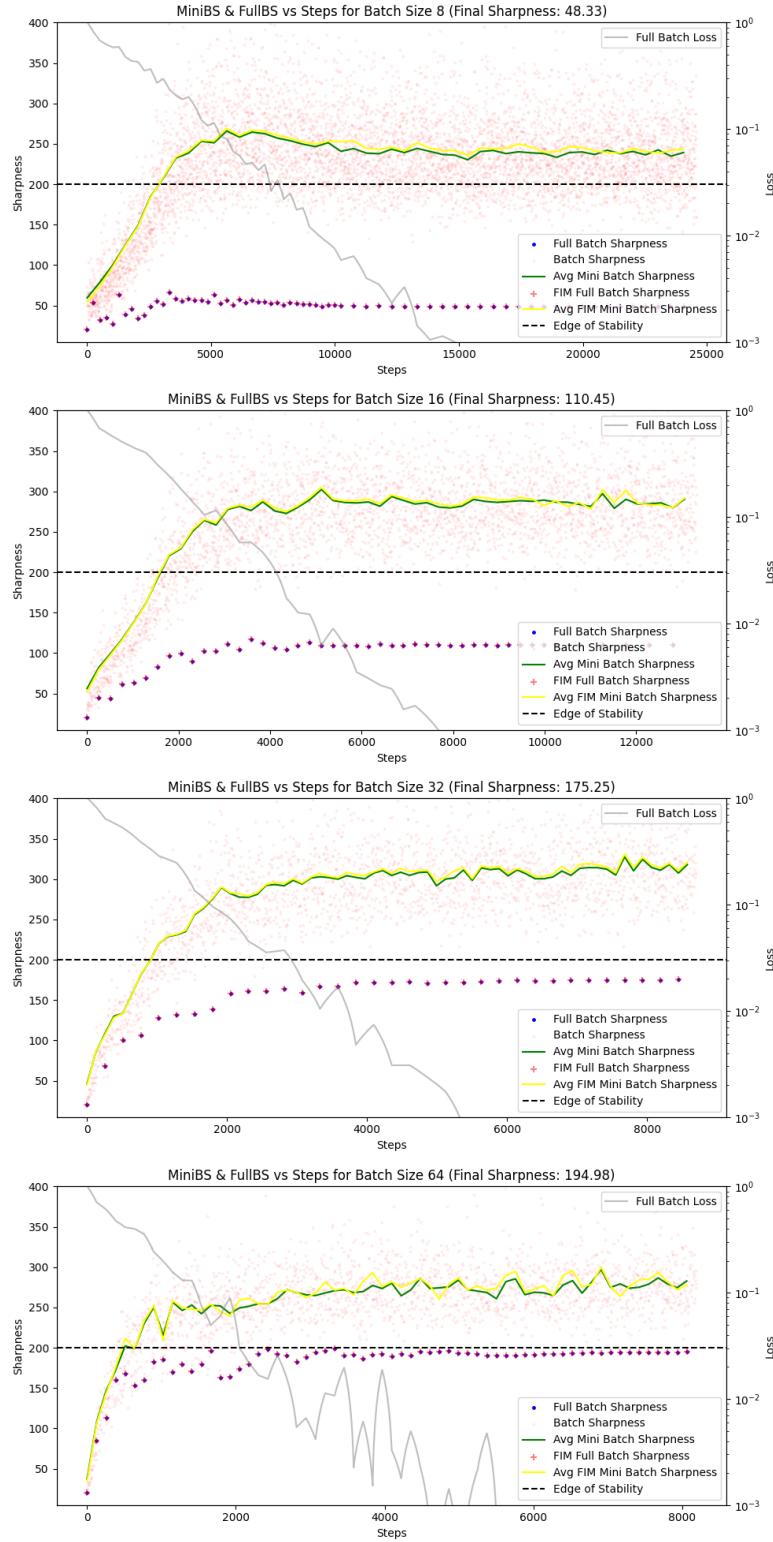


Figure 16. Ranging different batch sizes, the λ_{\max}^b corresponds to the largest eigenvalue of the averaged mini-batch NTK and $\frac{1}{b} J_B^\top J_B$, which corresponds with the FIM in vision classification tasks.

I. Exemplification Through a Simplified Model

To elucidate what the size of the λ_{\max}^b , consider a simplified scenario involving a diagonal linear network trained on data from two orthogonal classes. Assume $(x, y) \in \mathbb{R}^2 \times \mathbb{R}$ is either $z_1 = ((1, 0), 1)$ or $z_2 = ((0, 1), -1)$ with probability $1/2$. We learn this data with a diagonal linear network and MSE, precisely where

$$f(x) = a^\top B \cdot x, \quad a \in \mathbb{R}^2, \quad B \in \mathbb{R}^{2 \times 2}.$$

Then with a diagonal initialization, gradient descent will converge almost surely to a neural network of the following kind

$$f(x) = (a_1, a_2) \cdot \begin{pmatrix} b_1 & 0 \\ 0 & b_2 \end{pmatrix} \cdot x, \quad \text{where } |a_1 \cdot b_1| = |a_2 \cdot b_2| = 1.$$

At convergence, the spectrum of the Hessian on the data point z_1 is $\{\lambda_1, 0, 0, 0, 0, 0\}$, with $\lambda_1 := a_1^2 + b_1^2$, the Hessian on the data point z_2 is instead $\{\lambda_2, 0, 0, 0, 0, 0\}$, where $\lambda_2 := a_2^2 + b_2^2$, and the two eigenvectors for these two eigenvalues are orthogonal between each other. This implies that the Hessian of the full-batch loss has spectrum $\{\lambda_1/2, \lambda_2/2, 0, 0, 0, 0\}$, while the Hessian on the mini batches of size one has either one of the spectra above.

This implies that

$$\lambda_{\max} = \lambda_{\max} \left(\frac{1}{2} \mathcal{H}(z_1) + \frac{1}{2} \mathcal{H}(z_2) \right) = \max \left\{ \frac{\lambda_1}{2}, \frac{\lambda_2}{2} \right\} \quad (22)$$

This is smaller than the average largest eigenvalue of the mini-batch Hessian which is

$$\lambda_{\max}^1 = \frac{1}{2} \lambda_{\max}(\mathcal{H}(z_1)) + \frac{1}{2} \lambda_{\max}(\mathcal{H}(z_2)) = \frac{\lambda_1}{2} + \frac{\lambda_2}{2}. \quad (23)$$

- **Smaller size:** Thus setting λ_{\max} equal to λ means that the max between λ_1 and λ_2 is exactly 2λ . Note that the fact that $a_1 \cdot b_1 = a_2 \cdot b_2 = 1$ and Cauchy-Schwartz imply that $\lambda_1, \lambda_2 \geq 2$. Setting λ_{\max}^1 to λ thus implies that the maximum between λ_1 and λ_2 is *at most* $2\lambda - 2$, generally smaller.
- **Higher alignment:** Moreover, we have that the gradient $\nabla f(z_i)$ on the data point z_i exactly aligns with the eigenvector v_i of the highest eigenvalue λ_i of the Hessian in z_i . On the full batch, we are averaging them differently, precisely we have that there exist two constants c_1, c_2 such that the gradient is $\frac{c_1}{2} v_1 + \frac{c_2}{2} v_2$. Thus, where WLOG $\lambda_1 > \lambda_2$ we have the alignments

$$\mathcal{H}(z_1) \cdot \nabla L(z_1) \sim c_1 \lambda_1^2 v_1 \quad \text{but} \quad \mathcal{H} \cdot \nabla f \sim \frac{c_1}{2} \lambda_1^2 v_1 \quad (24)$$

Thus one half of it (batch size divided by number of data points).

This shows that in the same point of the gradient, SGD perceives the largest eigenvalue of the Hessian bigger and more relevant to the gradient than GD.

J. Illustration of EOSS in Variety of Settings: *Batch Sharpness*

In this appendix, we provide further empirical evidence that EOSS arises robustly across a variety of models, step sizes, and batch sizes. Consistent with our main observations, we find that *Batch Sharpness* invariably stabilizes around $2/\eta$.

MLP (2-Layer) Baseline. Figure 20 illustrates EOSS for our baseline network, an MLP with two hidden layers of dimension 512, trained on an 8192-sample subset of CIFAR-10 with step size $\eta = 0.004$. As the training proceeds, *Batch Sharpness* stabilizes around $2/\eta$, whereas λ_{\max} plateaus strictly below *Batch Sharpness*. Decreasing the step size to $\eta = 0.002$ (see Figure 17) rescales the plateau of *Batch Sharpness* around the new threshold $2/\eta$, in line with the behavior discussed in the main text.

5-Layer CNN. We further confirm the EOSS regime in a five-layer CNN. As depicted in Figures 24 and 18, *Batch Sharpness* continues to plateau near the instability threshold for two distinct step sizes, while λ_{\max} once again settles at a lower level. Notably, as we vary the batch size, the gap between *Batch Sharpness* and λ_{\max} increases for smaller batches, mirroring the patterns described in Section 5.

ResNet-14. Finally, we demonstrate that the EOSS regime also emerges for a canonical architecture commonly used in computer vision: RESNET-14. Note that we are using a version without Batch Normalization. Figure 19 highlights the same qualitative behavior, with *Batch Sharpness* stabilizing at $2/\eta$.

Overall, these experiments provide further confirmation that EOSS is a robust phenomenon across different architectures, step sizes, and batch sizes.

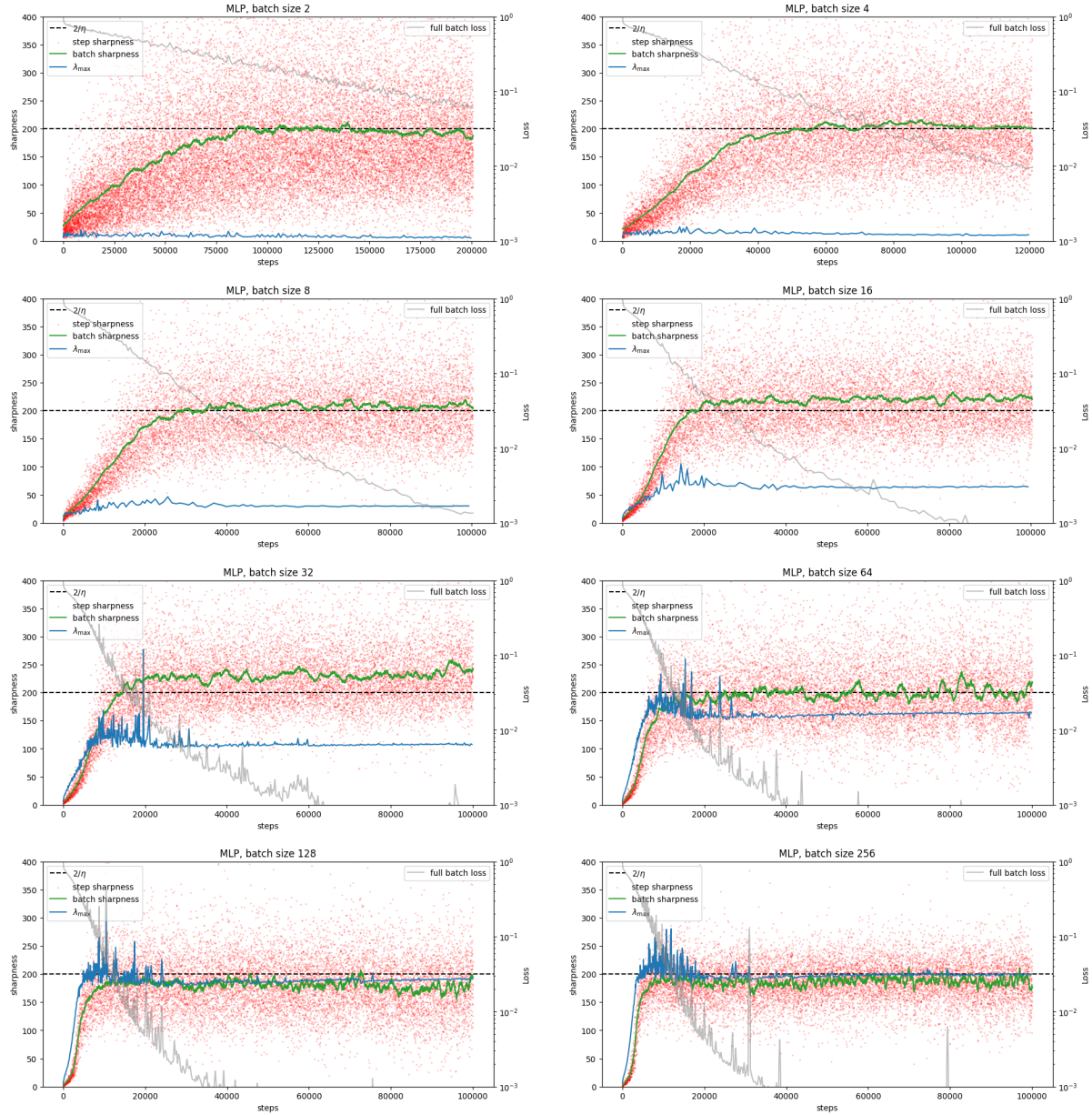


Figure 17. MLP: 2 hidden layers, hidden dimension 512; learning rate 0.01, 8k subset of CIFAR-10. Comparison between: the observed highest eigenvalue for the Hessian of the mini-batch loss (red dots), the empirical *Batch Sharpness* (green line), the λ_{\max} (blue dots).

Edge of Stochastic Stability

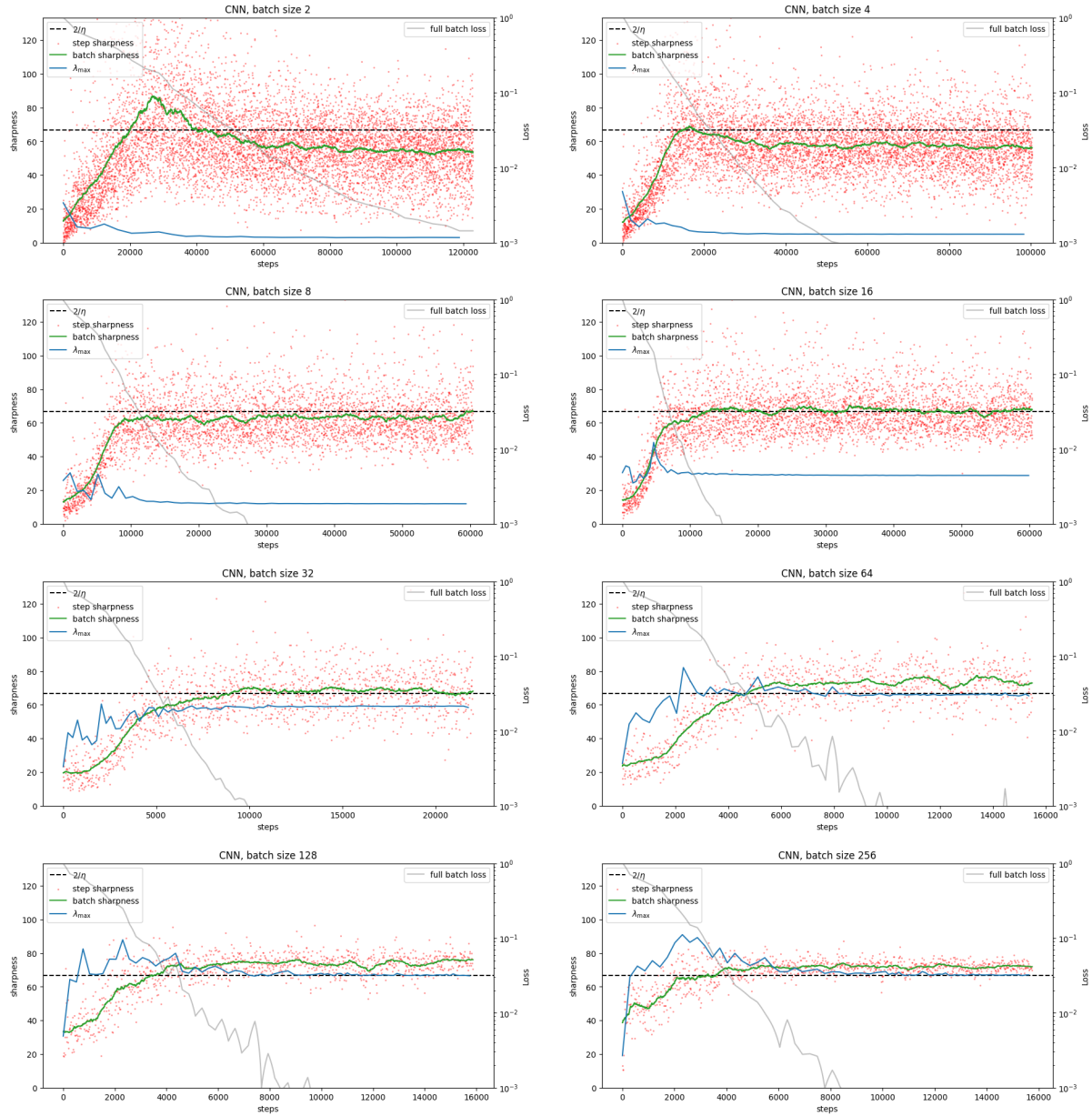


Figure 18. CNN: 5 layers (3 convolutional, 2 fully-connected), learning rate 0.03, 8k subset of CIFAR-10. Comparison between: the observed highest eigenvalue for the Hessian of the mini-batch loss (red dots), the empirical *Batch Sharpness* (green line), the λ_{\max} (blue dots).

Edge of Stochastic Stability

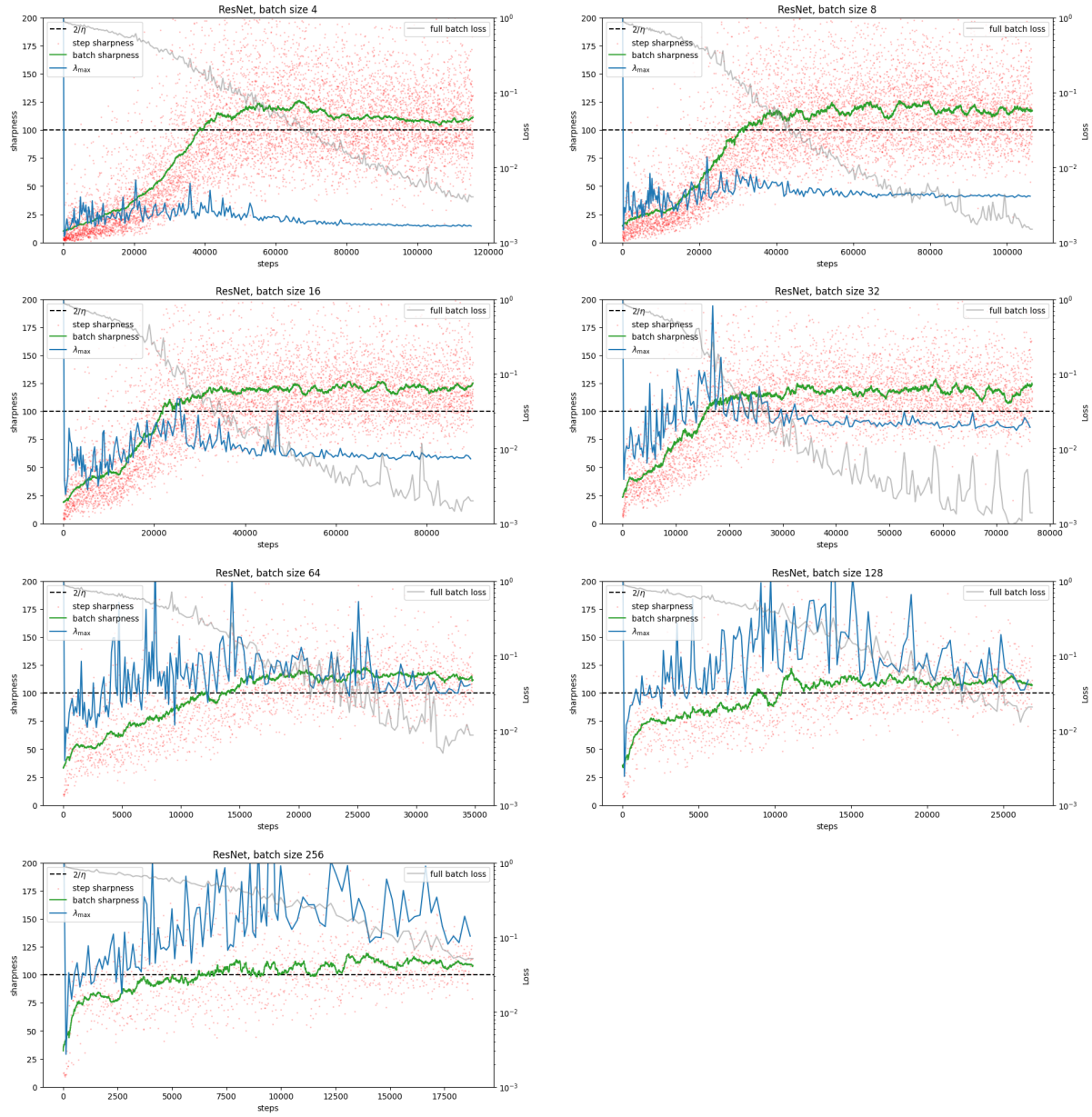


Figure 19. **ResNet-10**, learning rate 0.005, 8k subset of CIFAR-10. Comparison between: the observed highest eigenvalue for the Hessian of the mini-batch loss (red dots), the empirical *Batch Sharpness* (green line), the λ_{\max} (blue dots).

K. Illustration of EOSS in Variety of Settings: λ_{\max}^b

In this appendix, we provide further empirical evidence that EOSS arises robustly across a variety of models, step sizes, and batch sizes. Consistent with our main observations, we find that λ_{\max}^b invariably stabilizes within the interval $[2/\eta, 2 \times 2/\eta]$, while λ_{\max} remains strictly below λ_{\max}^b , with a gap that widens as the batch size decreases.

MLP (2-Layer) Baseline. Figure 20 illustrates EOSS for our baseline network, an MLP with two hidden layers of dimension 512, trained on an 8192-sample subset of CIFAR-10 with step size $\eta = 0.004$. As the training proceeds, λ_{\max}^b stabilizes in the range $[2/\eta, 2 \times 2/\eta]$, whereas λ_{\max} plateaus strictly below λ_{\max}^b . Decreasing the step size to $\eta = 0.002$ (see Figure 21) rescales the plateau of λ_{\max}^b around the new threshold $2/\eta$, in line with the behavior discussed in the main text.

Deeper MLP (4-Layer). To assess whether increased depth alters the phenomenon, we use a deeper MLP (MLP_L) with four hidden layers, training again on the same CIFAR-10 subset. Figures 22 and 23 show that λ_{\max}^b exhibits the same EOSS behavior for two different step sizes, reinforcing that depth alone does not invalidate our findings.

5-Layer CNN. We further confirm the EOSS regime in a five-layer CNN. As depicted in Figures 24 and 25, λ_{\max}^b continues to plateau near the instability threshold for two distinct step sizes, while λ_{\max} once again settles at a lower level. Notably, as we vary the batch size, the gap between λ_{\max}^b and λ_{\max} increases for smaller batches, mirroring the patterns described in Section 5.

ResNet-10. Finally, we demonstrate that the EOSS regime also emerges for a canonical architecture commonly used in computer vision: RESNET-10. Figure 26 highlights the same qualitative behavior, with λ_{\max}^b stabilizing at $[2/\eta, 2 \times 2/\eta]$ and λ_{\max} remaining consistently below λ_{\max}^b .

Overall, these experiments provide further confirmation that EOSS is a robust phenomenon across different architectures, step sizes, and batch sizes. Although the specific magnitude of λ_{\max} and the exact “hovering” value of λ_{\max}^b can vary, the overarching pattern of $\lambda_{\max}^b \approx 2/\eta$ and $\lambda_{\max} < \lambda_{\max}^b$ persists in all our tested settings.

Edge of Stochastic Stability

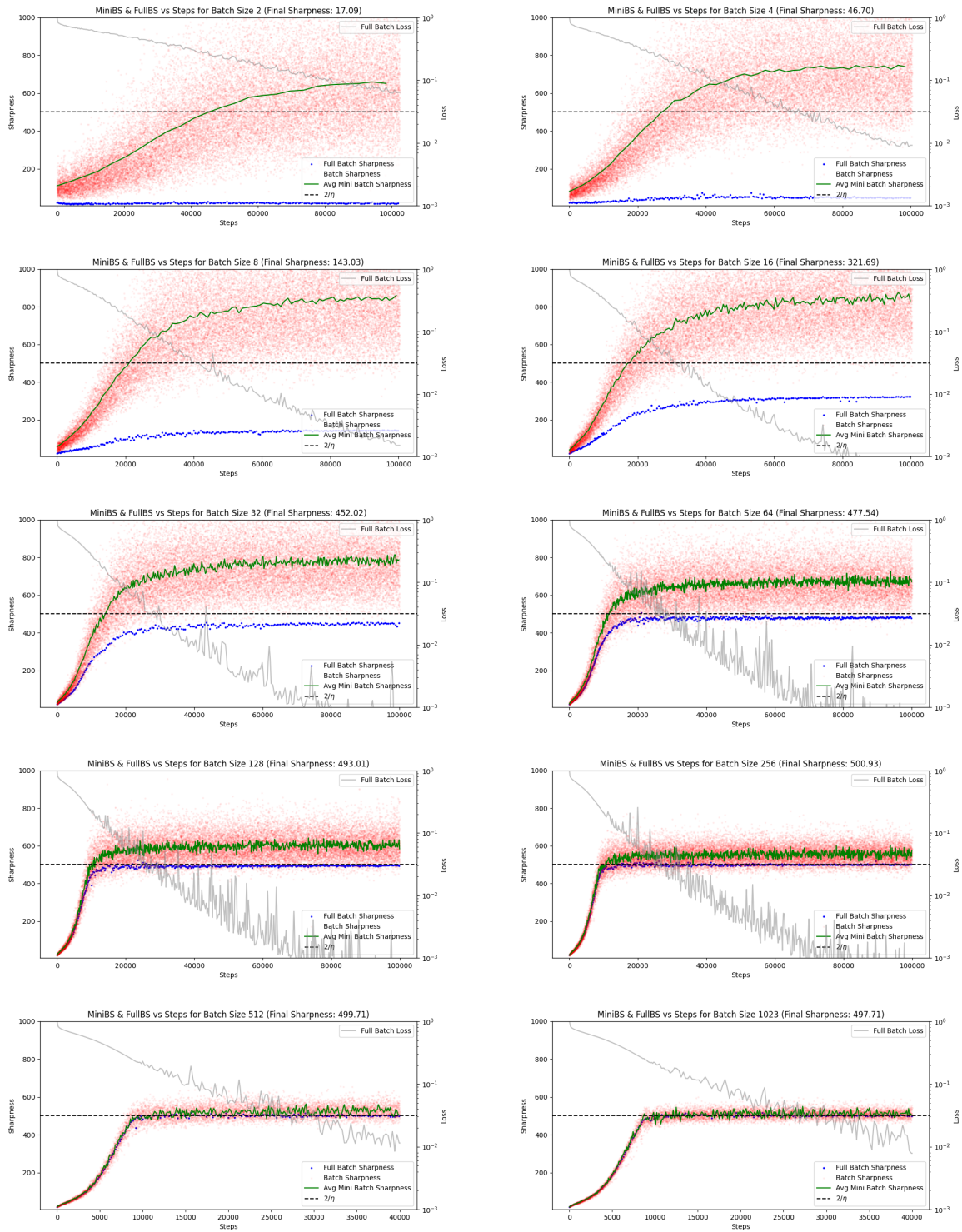


Figure 20. MLP, 2 hidden layers, hidden dimension 512, learning rate 0.004, 8k subset of CIFAR-10. Comparison between: the observed highest eigenvalue for the Hessian of the mini-batch loss (red dots), the empirical λ_{\max}^b (green line), the λ_{\max} (blue dots).

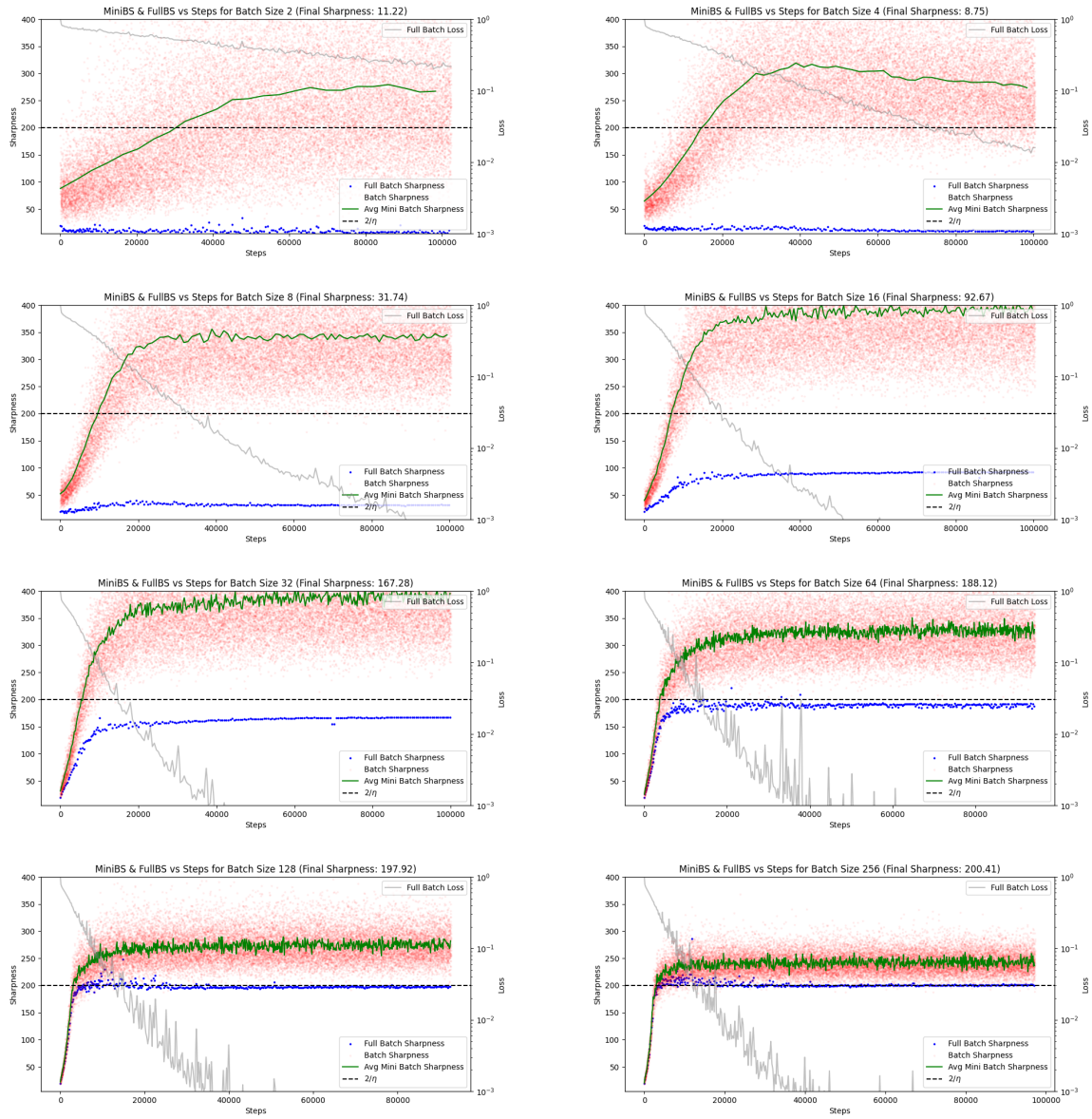


Figure 21. MLP: 2 hidden layers, hidden dimension 512; learning rate 0.01, 8k subset of CIFAR-10. Comparison between: the observed highest eigenvalue for the Hessian of the mini-batch loss (red dots), the empirical λ_{\max}^b (green line), the λ_{\max} (blue dots).

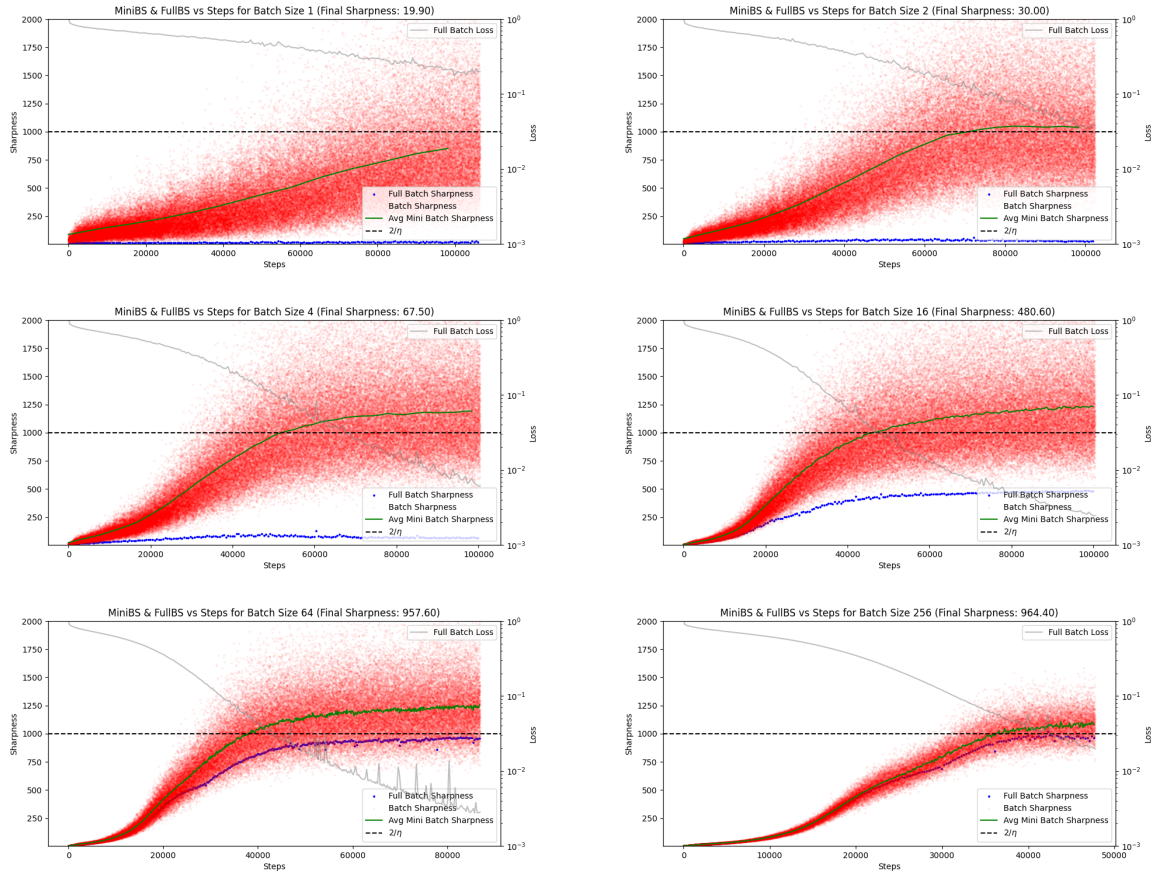


Figure 22. MLP_L: 4 hidden layers, hidden dimension 512, learning rate 0.002, 8k subset of CIFAR-10. Comparison between: the observed highest eigenvalue for the Hessian of the mini-batch loss (red dots), the empirical λ_{\max}^b (green line), the λ_{\max} (blue dots).

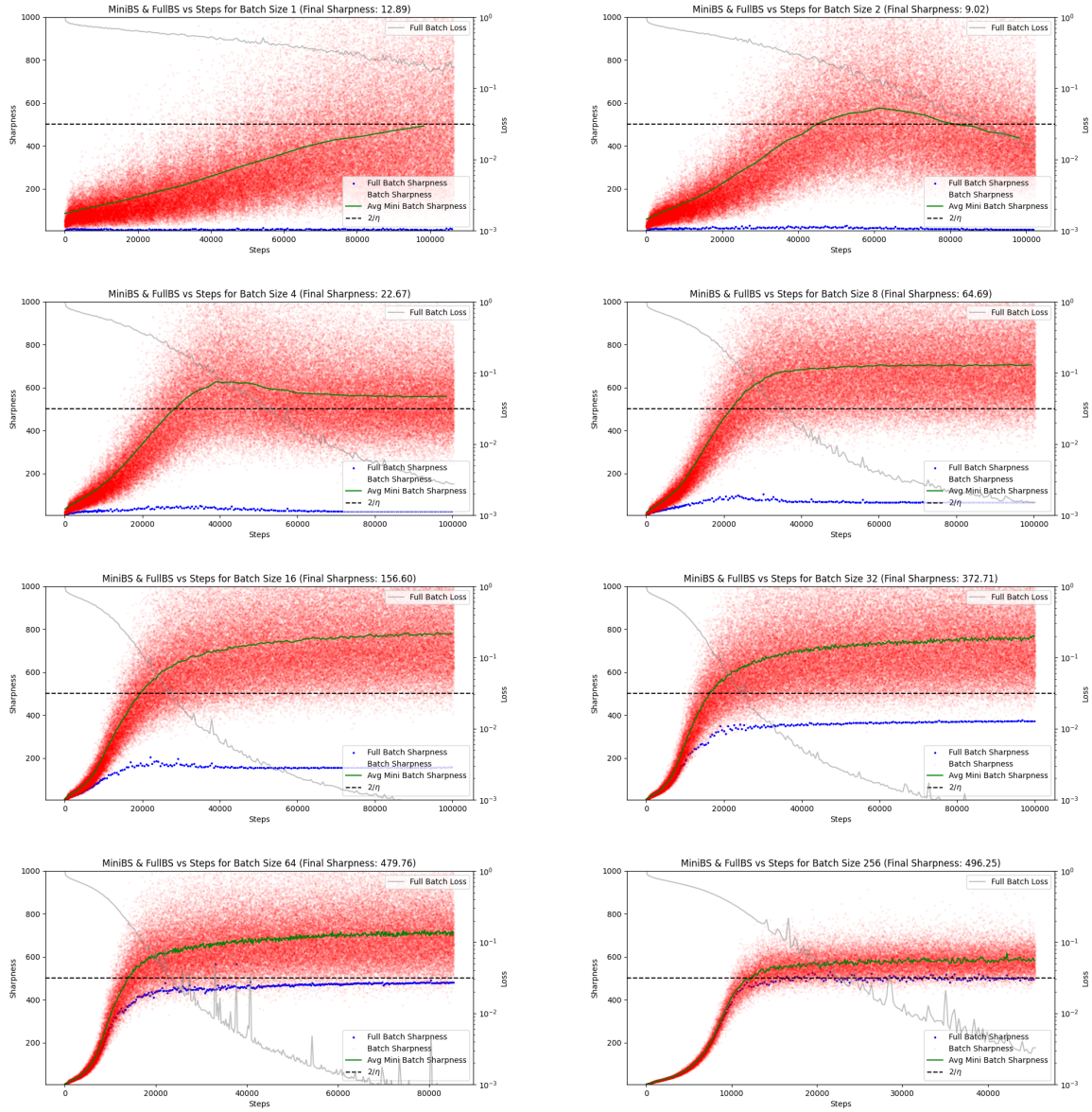


Figure 23. MLP_L, 4 hidden layers, hidden dimension 512, learning rate 0.004, 8k subset of CIFAR-10. Comparison between: the observed highest eigenvalue for the Hessian of the mini-batch loss (red dots), the empirical λ_{\max}^b (green line), the λ_{\max} (blue dots).

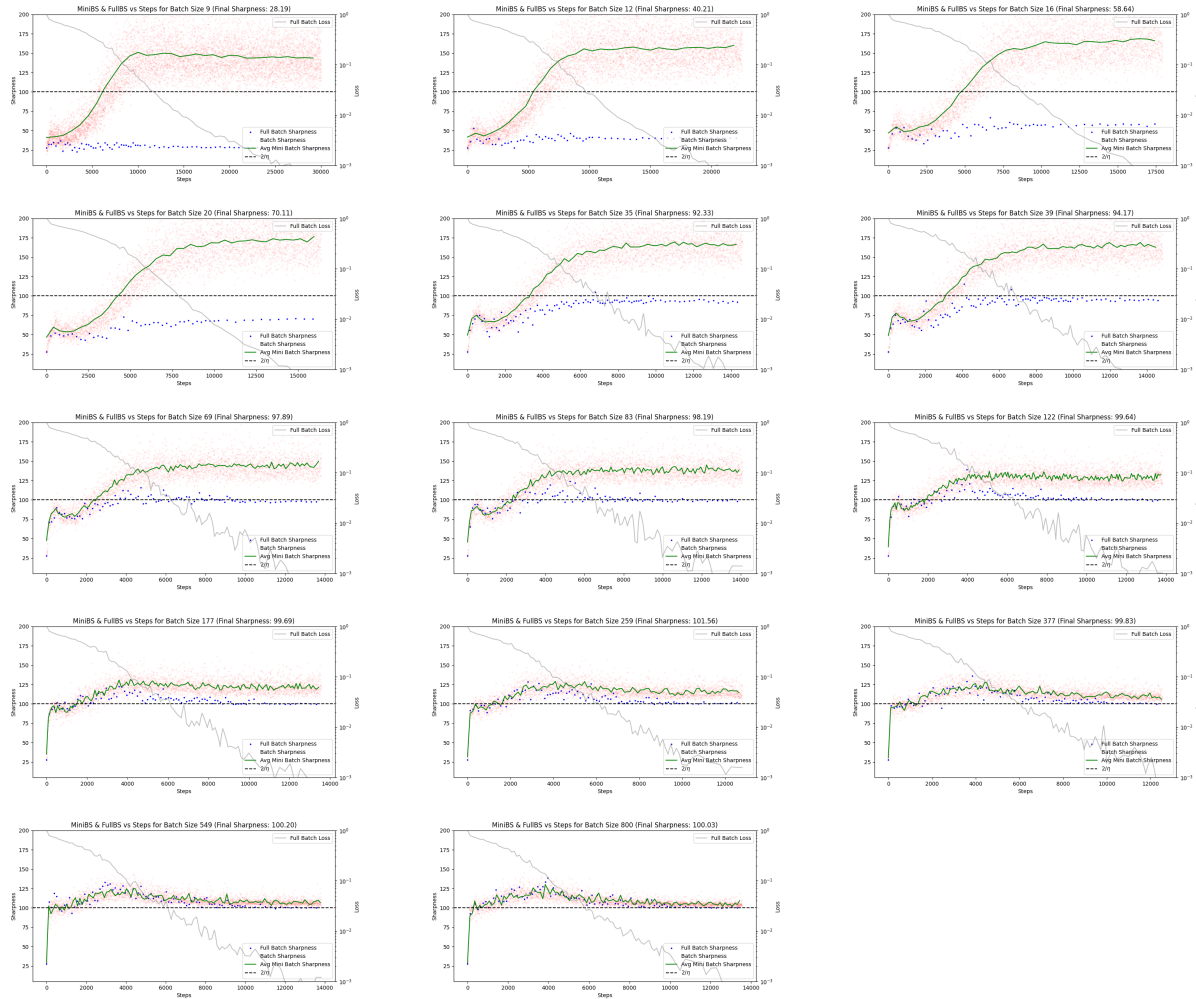


Figure 24. CNN, 5 layers (3 convolutional, 2 fully-connected), learning rate 0.02, 8k subset of CIFAR-10. Comparison between: the observed highest eigenvalue for the Hessian of the mini-batch loss (red dots), the empirical λ_{\max}^b (green line), the λ_{\max} (blue dots).

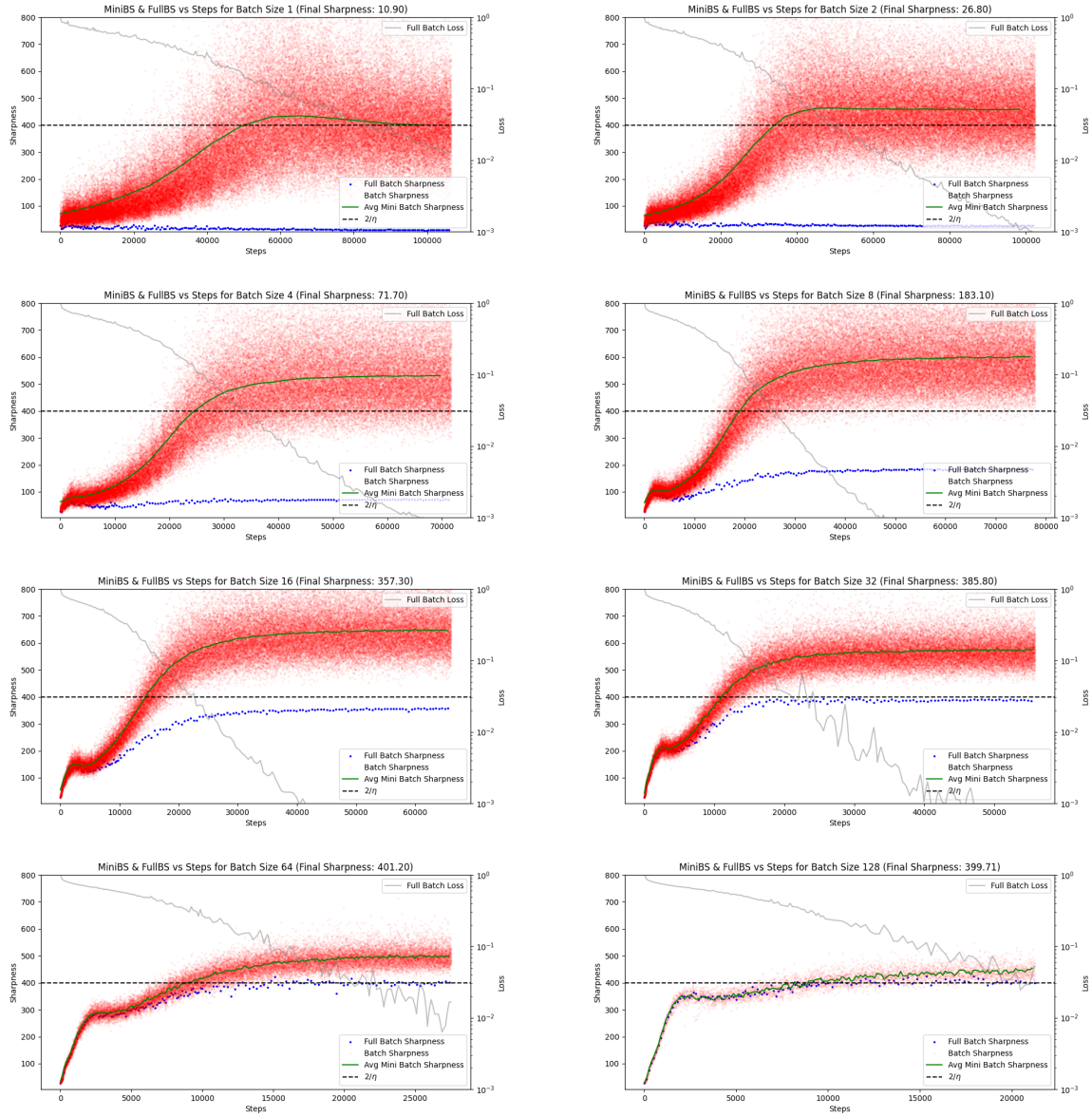


Figure 25. CNN, 5 layers (3 convolutional, 2 fully-connected), **learning rate 0.005**, 8k subset of CIFAR-10. Comparison between: the observed highest eigenvalue for the Hessian of the mini-batch loss (red dots), the empirical λ_{\max}^b (green line), the λ_{\max} (blue dots).

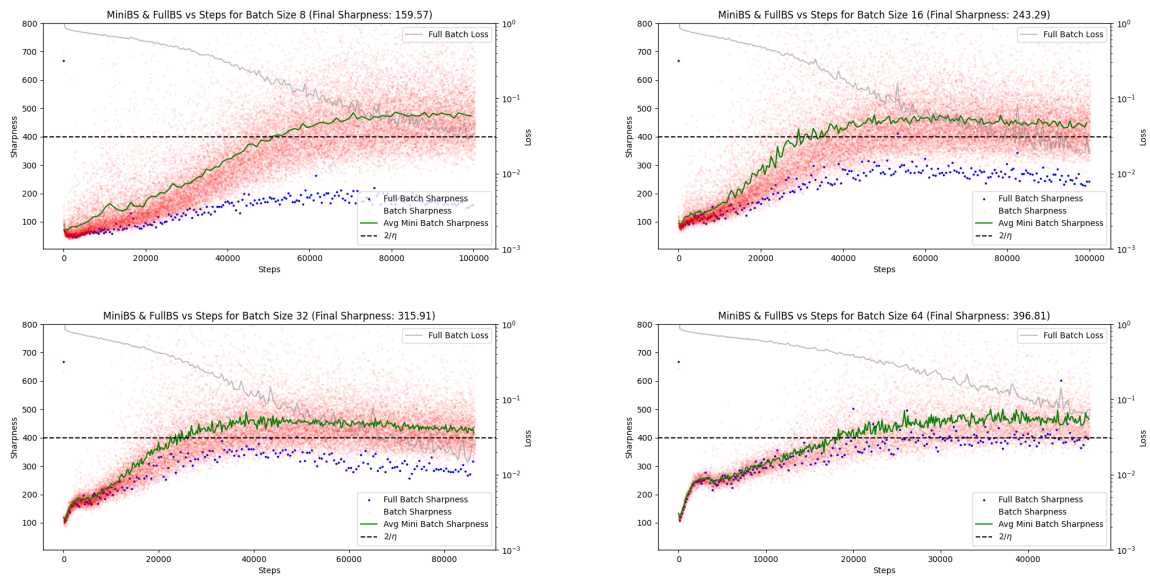


Figure 26. ResNet-10, learning rate 0.005, 8k subset of CIFAR-10. Comparison between: the observed highest eigenvalue for the Hessian of the mini-batch loss (red dots), the empirical λ_{\max}^b (green line), the λ_{\max} (blue dots).